

# We are IntechOpen, the world's leading publisher of Open Access books Built by scientists, for scientists

6,900

Open access books available

186,000

International authors and editors

200M

Downloads

Our authors are among the

154

Countries delivered to

TOP 1%

most cited scientists

12.2%

Contributors from top 500 universities



WEB OF SCIENCE™

Selection of our books indexed in the Book Citation Index  
in Web of Science™ Core Collection (BKCI)

Interested in publishing with us?  
Contact [book.department@intechopen.com](mailto:book.department@intechopen.com)

Numbers displayed above are based on latest data collected.  
For more information visit [www.intechopen.com](http://www.intechopen.com)



---

# A Simplified Analytical Method for High-Rise Buildings

---

Hideo Takabatake

Additional information is available at the end of the chapter

<http://dx.doi.org/10.5772/51158>

---

## 1. Introduction

High-rise buildings are constructed everywhere in the world. The height and size of high-rise buildings get larger and larger. The structural design of high-rise buildings depends on dynamic analysis for winds and earthquakes. Since today performance of computer progresses remarkably, almost structural designers use the software of computer for the structural design of high-rise buildings. Hence, after that the structural plane and outline of high-rise buildings are determined, the structural design of high-rise buildings which checks structural safety for the individual structural members is not necessary outstanding structural ability by the use of structural software on the market. However, it is not exaggeration to say that the performance of high-rise buildings is almost determined in the preliminary design stages which work on multifaceted examinations of the structural form and outline. The structural designer is necessary to gap exactly the whole picture in this stage. The static and dynamic structural behaviors of high-rise buildings are governed by the distributions of transverse shear stiffness and bending stiffness per each storey. Therefore, in the preliminary design stages of high-rise buildings a simple but accurate analytical method which reflects easily the structural stiffness on the whole situation is more suitable than an analytical method which each structural member is indispensable to calculate such as FEM.

There are many simplified analytical methods which are applicable for high-rise buildings. Since high-rise buildings are composed of many structural members, the main treatment for the simplification is to be replaced with a continuous simple structural member equivalent to the original structures. This equivalently replaced continuous member is the most suitable to use the one-dimensional rod theory.

Since the dynamic behavior of high-rise buildings is already stated to govern by the shear stiffness and bending stiffness determined from the structural property. The deformations of high-rise buildings are composed of the axial deformation, bending deformation, transverse

shear deformation, shear-lag deformation, and torsional deformation. The problem is to be how to take account of these deformations under keeping the simplification.

There are many rod theories. The most simple rod theory is Bernonlli-Euler beam theory which may treat the bending deformation excluding the transverse shear deformation. The Bernonlli-Euler beam theory is unsuitable for the modeling of high-rise buildings.

The transverse resistance of the frame depends on the bending of each structural member consisted of the frame. Therefore, the transverse deformation always occurs corresponding to the transverse stiffness  $\kappa GA$ . Since the transverse shear deformation is independent of the bending deformation of the one-dimensional rod, this shear deformation cannot neglect as for equivalent rod theory. This deformation behavior can be expressed by Timoshenko beam theory. Timoshenko beam theory may consider both the bending and the transverse shear deformation of high-rise buildings. The transverse deformation in Timoshenko beam theory is assumed to be linear distributed in the transverse cross section.

Usual high-rise buildings have the form of the three-dimensional structural frame. Therefore the structures produce the three dimensional behaviors. The representative dissimilarity which is differ from behavior of plane frames is to cause the shear-lag deformation. The shear-lag deformation is noticed in bending problem of box form composed of thin-walled closed section.

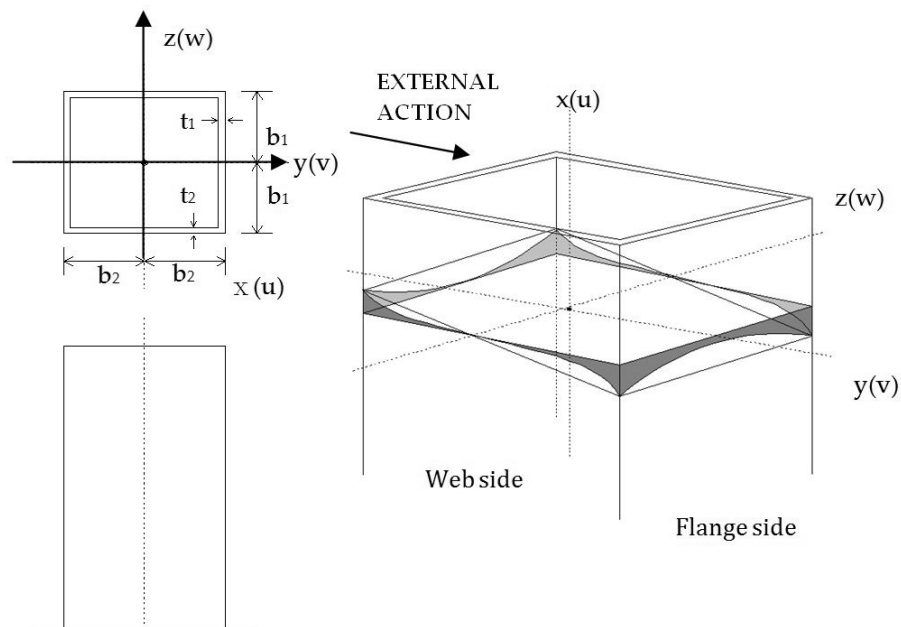
Reissner [1] presented a simplified beam theory including the effect of the shear-lag in the Bernonlli-Euler beam for bending problem of box form composed of thin-walled member. In this theory the shear-lag is considered only the flange of box form. This phenomenon appears in high-rise buildings the same as wing of aircrafts. Especially the shear-lag is remarkable in tube structures of high-rise buildings and occurs on the flange sides and web ones of the tube structures. The shear-lag occurs on all three-dimensional frame structures to a greater or lesser degree. Thus the one-dimensional rod theory which is applicable to analyze simply high-rise buildings is necessary to consider the longitudinal deformation, bending deformation, transverse shear deformation, shear-lag deformation, and torsional deformation. In generally, high-rise buildings have doubly symmetric structural forms from viewpoint the balance of facade and structural simplicity. Therefore the torsional deformation is considered to separate from the other deformations. Takabatake [2-6] presented a one-dimensional rod theory which can consider simply the above deformations. This theory is called the one-dimensional extended rod theory.

The previous works for continuous method are surveyed as follows: Beck [7] analyzed coupled shear walls by means of beam model. Heidenbrech et al. [8] indicated an approximate analysis of wall-frame structures and the equivalent stiffness for the equivalent beam. Dynamic analysis of coupled shear walls was studied by Tso et al. [9], Rutenberg [10, 11], Darnay et al. [12], and Bause [13]. Cheung and Swaddiwudhipong [14] presented free vibration of frame shear wall structures. Coull et al. [15, 16] indicated simplified analyses of tube structures subjected to torsion and bending. Smith et al. [17, 18] proposed an approximate method for deflections and natural frequencies of tall buildings. However, the aforementioned continuous approaches have not been presented as a closed-form solution for tube

structures with variable stiffness due to the variation of frame members and bracings. In this chapter high-rise buildings are expressed as tube structures in which three dimensional frame structures are included naturally.

## 2. Formulation of the one-dimensional extended rod theory for high-rise buildings

Frame tubes with braces and/or shear walls are replaced with an equivalent beam. Assuming that in-plane floor's stiffness is rigid, the individual deformations of outer and inner tubes in tube-in-tube are restricted. Hence, the difference between double tube and single tube depends on only the values of bending stiffness, transverse shear stiffness, and torsional stiffness. Therefore, for the sake of simplicity, consider a doubly symmetric single tube structure, as shown in Figure 1. Cartesian coordinate system,  $x, y, z$  is employed, in which the axis  $x$  takes the centroidal axis, and the transverse axes  $y$  and  $z$  take the principal axes of the tube structures. Since the lateral deformation and torsional deformation for a doubly symmetric tube structure are uncouple, the governing equations for these deformations can be formulated separately for simplicity.



**Figure 1.** Doubly symmetric tube structure

### 2.1. Governing equations for lateral forces

Consider a motion of the tube structure subjected to lateral external forces such as winds and earthquakes acting in the  $y$ -direction, as shown in Figure 1. The deformation of the tube structures is composed of axial deformation, bending, transverse shear deformation, and

shear-lag, in which the in-plane distortion of the cross section is neglected due to the in-plane stiffness of the slabs. The displacement composes  $\bar{U}(x, y, z, t)$ ,  $\bar{V}(x, y, z, t)$ , and  $\bar{W}(x, y, z, t)$  in the  $x$ -,  $y$ -, and  $z$ -directions on the middle surface of the tube structures as

$$\bar{U}(x, y, z, t) = u(x, t) + y\phi(x, t) + \varphi^*(y, z)u^*(x, t) \quad (1)$$

$$\bar{V}(x, y, z, t) = v(x, t) \quad (2)$$

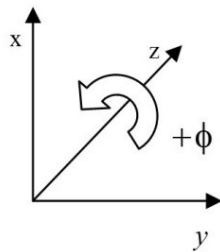
$$\bar{W}(x, y, z, t) = 0 \quad (3)$$

in which  $u$  and  $v$  = longitudinal and transverse displacement components in the  $x$ - and  $y$ -directions on the axial point, respectively;  $\phi$  = rotational angle on the axial point along the  $z$ -axis;  $u^*$  = shear-lag coefficient in the flanges;  $\varphi^*(x, y)$  = shear-lag function indicating the distribution of shear-lag. These displacements and shear-lag coefficient are defined positive as the positive direction of the coordinate axes. However, the rotation is defined positive as counterclockwise along the  $z$  axis, as shown in Figure 2. The shear-lag function for the flange sections is used following function given by Reissner [1] and for the web sections sine distribution [5, 6] is assumed:

$$\varphi^*(y, z) = \pm \left[ 1 - \left( \frac{z}{b_1} \right)^2 \right] \text{ for flange} \quad (4)$$

$$\varphi^*(y, z) = \sin\left(\frac{\pi y}{b_2}\right) \text{ for web} \quad (5)$$

in which the positive of  $\pm$  takes for the flange being the positive value of the  $y$ -axis and vice versa  $b_1$  and  $b_2$  are half width of equivalent flange and web sections, as shown in Figure 1.



**Figure 2.** Positive direction of rotation  $\phi$

The governing equation of tube structures is proposed by means of the following Hamilton's principle.

$$\delta I = \delta \int_{t_1}^{t_2} (T - U - V) dt = 0 \quad (6)$$

in which  $T$  = the kinetic energy;  $U$  = the strain energy;  $V$  = the potential energy produced by the external loads; and  $\delta$  = the variational operator taken during the indicated time interval.

Using linear relationship between strain and displacement, the following expressions are obtained.

$$\varepsilon_x = \frac{\partial \bar{U}}{\partial x} = u' + y\phi' + \varphi^* u^{*'} \quad (7)$$

$$\gamma_{xy} = \frac{\partial \bar{U}}{\partial y} + \frac{\partial \bar{V}}{\partial x} = \phi + \varphi^*_{,y} u^* + v' \quad (8)$$

$$\gamma_{xz} = \frac{\partial \bar{U}}{\partial z} + \frac{\partial \bar{W}}{\partial x} = \varphi^*_{,z} u^* \quad (9)$$

in which dashes indicate the differentiation with respect  $x$  and the differentiations with respect  $y$  and  $z$  are expressed as

$$\varphi^*_{,y} = \frac{\partial \varphi^*}{\partial y} \quad (10)$$

$$\varphi^*_{,z} = \frac{\partial \varphi^*}{\partial z} \quad (11)$$

The relationships between stress and strain are used well-known engineering expression for one-dimensional structural member of the frame structure.

$$\sigma_x = E \varepsilon_x \quad (12)$$

$$\tau_{xy} = G \gamma_{xy} \quad (13)$$

$$\tau_{xz} = G \gamma_{xz} \quad (14)$$

in which  $E$  is Young modulus and  $G$  shear modulus.

Assuming the above linear stress-strain relation, the strain energy  $U$  is given by

$$U = \frac{1}{2} \int_0^L [EA(u')^2 + EI(\phi')^2 + EI^*(u^{*'})^2 + \kappa GF^*(u^*)^2 + 2ES^*\phi'u^{*'} + \kappa GA(v' + \phi)^2] dx \quad (15)$$

in which  $L$  = the total height of the tube structure;  $k$  = the shear coefficient; and  $A$ ,  $I$ ,  $I^*$ ,  $S^*$ , and  $F^*$  = the sectional stiffnesses. These sectional stiffnesses vary discontinuously with respect to  $x$  for a variable tube structure and are defined as

$$A = \iint dydz = \sum A_c \quad (16)$$

$$I = \iint y^2 dydz \quad (17)$$

$$A^* = \iint \varphi^* dydz = \iint [\varphi_f^* + \varphi_w^*] dydz \quad (18)$$

$$I^* = \iint (\varphi^*)^2 dydz = 2t_2 \int_{-b_1}^{b_1} (\varphi_f^*)^2 dz + 2t_1 \int_{-b_2}^{b_2} (\varphi_w^*)^2 dy \quad (19)$$

$$S^* = \iint y \varphi^* dydz = 2t_2 \int_{-b_1}^{b_1} b_2 \varphi_f^* dz + 2t_1 \int_{-b_2}^{b_2} y \varphi_w^* dy \quad (20)$$

$$F^* = \iint (\varphi_{,z}^*)^2 dydz + \iint (\varphi_{,y}^*)^2 dydz = \iint (\varphi_{f,z}^* + \varphi_{w,z}^*)^2 dydz + \iint (\varphi_{f,y}^* + \varphi_{w,y}^*)^2 dydz \quad (21)$$

in which  $\sum A_c$  = the total cross-sectional area of columns per story.

The kinetic energy,  $T$ , for the time interval from  $t_1$  to  $t_2$  is

$$T = \int_{t_1}^{t_2} \left\{ \frac{1}{2} \int_0^L [\rho A (\dot{u})^2 + \rho I (\dot{\phi})^2 + \rho I^* (\dot{u}^*)^2 + 2\rho S^* \dot{\phi} \dot{u}^* + \rho A (\dot{v})^2] dx \right\} dt \quad (22)$$

in which the dot indicates differentiation with respect to time and  $\rho$  = mass density of the tube structure. Now assuming that the variation of the displacements and rotation at  $t=t_1$  and  $t=t_2$  is negligible, the variation  $\delta T$  may be written as

$$\delta T = - \int_{t_1}^{t_2} \left\{ \int_0^L [\rho A \ddot{u} \delta u + \rho I \ddot{\phi} \delta \phi + \rho I^* \ddot{u}^* \delta u^* + \rho S^* (\ddot{\phi} \delta u^* + \ddot{u}^* \delta \phi) + \rho A \ddot{v} \delta v] dx \right\} dt \quad (23)$$

When the external force at the boundary point (top for current problem) prescribed by the mechanical boundary condition is absent, the variation of the potential energy of the tube structures becomes

$$\delta V = - \int_0^L \left[ \iint (p_x \delta \bar{U} + p_y \delta \bar{V}) dydz \right] dx + \int_0^L (c_u \dot{u} \delta u + c_v \dot{v} \delta v) dx \quad (24)$$

in which  $p_x$  and  $p_y$  = components of external loads in the  $x$ - and  $y$ -directions per unit are, respectively;  $c_u$ , and  $c_v$  = damping coefficients for longitudinal and transverse motions, respectively. The substitution of Eqs. (1) and (2) into Eq. (24) yields

$$\delta V = - \int_0^L (P_x \delta u + m \delta \phi + m^* \delta u^* + P_y \delta v - c_u \dot{u} \delta u - c_v \dot{v} \delta v) dx \quad (25)$$

in which  $P_x$ ,  $P_y$ ,  $m$ , and  $m^*$  are defined as

$$P_x = \iint p_x dy dz \quad (26)$$

$$P_y = \iint p_y dy dz \quad (27)$$

$$m = \iint p_x y dy dz \quad (28)$$

$$m^* = \iint p_x \phi^* dy dz = 0 \quad (29)$$

Since for a doubly symmetric tube structure the distribution of the shear-lag function on the flange and web surfaces confronting each other with respect to  $z$  axis is asymmetric,  $m^*$  vanishes. Hence, Eq. (25) reduces to

$$\delta V = - \int_0^L (P_x \delta u + m \delta \phi + P_y \delta v - c_u \dot{u} \delta u - c_v \dot{v} \delta v) dx \quad (30)$$

Substituting Eqs. (15), (28), and (30) into Eq. (6), the differential equations of motion can be obtained

$$\delta u : \rho A \ddot{u} + c_u \dot{u} - (EA u')' - P_x = 0 \quad (31)$$

$$\delta v : \rho A \ddot{v} + c_v \dot{v} - [\kappa GA (v' + \phi)]' - P_y = 0 \quad (32)$$

$$\delta \phi : \rho I \ddot{\phi} + \rho S^* \ddot{u}^* - (EI \phi' + ES^* u^*)' + \kappa GA (v' + \phi) - m = 0 \quad (33)$$

$$\delta u^* : \rho I^* \ddot{u}^* + \rho S^* \ddot{\phi} - (EI^* u^{*'} + ES^* \phi')' + \kappa GF^* u^* = 0 \quad (34)$$

together with the associated boundary conditions at  $x=0$  and  $x=L$ .



$$u = 0 \text{ or } EAu' = 0 \quad (35)$$

$$v = 0 \text{ or } \kappa GA(v' + \phi) = 0 \quad (36)$$

$$\phi = 0 \text{ or } EI\phi' + ES^*u^{*'} = 0 \quad (37)$$

$$u^* = 0 \text{ or } EI^*u^{*'} + ES^*\phi' = 0 \quad (38)$$

## 2.2. Governing equations for torsional moment

The displacement components for current tube structures subjected to torsional moments,  $m_x$ , around the  $x$ -axis are expressed by

$$\bar{U} = \bar{w}(y, z)\theta'(x, t) \quad (39)$$

$$\bar{V} = -z\theta \quad (40)$$

$$\bar{W} = y\theta \quad (41)$$

in which  $\bar{W}$  = the displacement component in the  $z$ -direction on the tube structures;  $\theta$  = torsional angle; and  $\bar{w}(y, z)$  = warping function. Using the same manner as the aforementioned development, the differential equation of motion for current tube structures can be obtained

$$\delta\theta : \rho I_p \ddot{\theta} - (GJ\theta')' - m_x = 0 \quad (42)$$

together with the association boundary conditions

$$\theta = 0 \text{ or } GJ\theta' = m_{xL} \quad (43)$$

at  $x=0$  and  $L$ , in which  $GJ$  = the torsional stiffness.

## 2.3. Sectional constants

The sectional constants are defined by Eqs. (16) to (21). For doubly symmetric single-tube structures as shown in Figure 1, these sectional constants are simplified as follow.

$$A^* = 0 \quad (44)$$

$$I^* = \frac{8}{15}A_f + \frac{1}{2}A_w \quad (45)$$

$$S^* = \frac{2}{3}b_2A_f + \frac{b_2}{\pi}A_w \quad (46)$$

$$F^* = \frac{4}{3(b_1)^2}A_f + \frac{\pi^2}{2b_2^2}A_w \quad (47)$$

in which  $A_f$  = the total cross-sectional area of columns in the flanges and webs, respectively, per story. For the cross-section of tube structures, as shown in Figure 1,  $A_f$  and  $A_w$  are given as  $A_f = 4t_1b_1$  and  $A_w = 4t_2b_2$ .

#### 2.4. Equivalent transverse shear stiffness $\kappa GA$

When the tube structure are composed of frame and bracing, the equivalent transverse shear stiffness  $\kappa GA$  for each story is given by

$$\kappa GA = \sum (\kappa GA)_{frame} + \sum (\kappa GA)_{brace} \quad (48)$$

in which  $\sum$  is taken the summation of equivalent transverse shear stiffnesses of web frame and of braces per story. The shear stiffnesses of web frame and web double-brace  $\sum (\kappa GA)_{frame}$  and  $\sum (\kappa GA)_{brace}$  for each side of the web surfaces, respectively, are given by

$$\frac{1}{(\kappa GA)_{frame}} = \frac{h \left( \frac{1}{\sum K_c} + \frac{1}{\sum K_b} \right)}{12E} + \frac{1}{\sum_c (\kappa GA_{cw})} + \frac{h}{\sum_b (\ell \kappa GA_{bw})} \quad (49)$$

$$(\kappa GA)_{brace} = \frac{h}{\ell} k_{brace} A_B E_B \cos^2 \theta_B \quad (50)$$

in which the first term on the right side of Eq. (49) indicates the deformation of the frame with the stiffnesses of columns and beams  $K_c$  and  $K_b$ , respectively; the second and third terms indicate the shear deformation of only the columns and beams in the current web-frame, respectively.  $A_{cw}$  and  $A_{bw}$  = the web's cross-sectional area of a column and of a beam, respectively.  $\sum_c$  and  $\sum_b$  = the sums of columns and beams, respectively, in a web-frame at the current story of the frame tube. If the shear deformations of columns and beams are neglected, these terms must vanish. Furthermore,  $\ell$  = the span length;  $A_B$  = the cross-sectional area of a brace;  $E_B$  = the Young's modulus; and  $\theta_B$  = the incline of the brace. The coefficient  $k_{brace}$  indicates the effective number of brace and takes  $k_{brace} = 1$  for a brace resisting only tension and  $k_{brace} = 2$  for two brace resisting tension and compression, as shown in Figure 3.

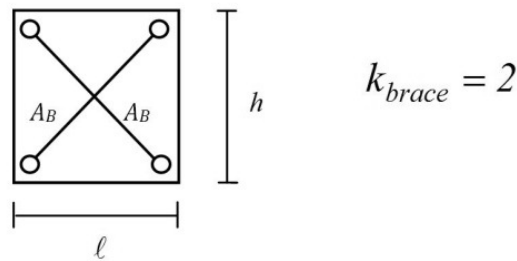


Figure 3. Brace resisting tension and compression

2.5. Equivalent bending stiffness  $EI$

The equivalent bending stiffness  $EI$  for each storey is determined from the total sum of the moment of inertia about the  $z$ -axis of each column located on the storey.

$$EI = \sum_{i=1}^n E_i [I_{0i} + A_i e_i^2] \tag{51}$$

in which  $E_i$ ,  $I_{0i}$  and  $A_i$  = Young modulus, moment of inertia and the cross section of the  $i$ th column; and  $e_i$  = the distance measured from the  $z$ -axis.

3. Static analysis by the finite defference method

3.1. Expression of static analysis

The governing equations for the one-dimensional extended rod theory are differential equations with variable coefficients due to the variation of structural members and forms in the longitudinal direction. Furthermore, although the equations of motion and boundary conditions for the vertical displacement  $u$  are uncoupled from the other displacement components, the governing equations take coupled from concerning variables  $v$ ,  $\phi$ , and  $u^*$ .

Takabatake [2, 3] presented the uncoupled equations as shown in section 7 by introducing positively appropriate approximations into the coupled equations and proposed a closed-form solution. For usual tube structures this method produces reasonable results. However the analytical approach deteriorates on the accuracy of numerical results for high-rise buildings with the rapid local variations of transverse shear stiffness and/or braces. Especially the difference appears on the distributions of not dynamic deflection but story acceleration and storey shear force. It is limit to express these rapid variations by a functional expression. So, the above governing equations are solved by means of the finite difference method.

The equations of motion and boundary conditions for the longitudinal displacement  $u$  are uncoupled from the other displacement components. So we consider only the lateral motion

given by the governing equation coupled about the lateral displacements  $v$ , rotational angle  $\phi$ , and shear-lag displacement  $u^*$ .

Using ordinary central finite differences, the finite difference expressions of the current equilibrium equations, obtained from the equations of motion Eqs. (32)-(34), may be written, respectively, as follows:

$$\begin{aligned} & \left[ -\frac{\kappa GA}{\Delta^2} + \frac{(\kappa GA)'}{2\Delta} \right] v_{i-1} + \frac{\kappa GA}{2\Delta} \phi_{i-1} + \frac{2\kappa GA}{\Delta^2} v_i \\ & - (\kappa GA)' \phi_i - \left[ \frac{\kappa GA}{\Delta^2} + \frac{(\kappa GA)'}{2\Delta} \right] v_{i+1} - \frac{\kappa GA}{2\Delta} \phi_{i+1} = P_{yi} \end{aligned} \quad (52)$$

$$\begin{aligned} & -\frac{\kappa GA}{2\Delta} v_{i-1} + \left[ -\frac{EI}{\Delta^2} + \frac{(EI)'}{2\Delta} \right] \phi_{i-1} + \left[ -\frac{ES^*}{\Delta^2} + \frac{(ES^*)'}{2\Delta} \right] u_{i-1}^* + \left( \frac{2EI}{\Delta^2} + \kappa GA \right) \phi_i \\ & + \frac{2ES^*}{\Delta^2} u_i^* + \frac{\kappa GA}{2\Delta} v_{i+1} + \left[ -\frac{EI}{\Delta^2} + \frac{(EI)'}{2\Delta} \right] \phi_{i+1} + \left[ -\frac{ES^*}{\Delta^2} - \frac{(ES^*)'}{2\Delta} \right] u_{i+1}^* = m_{zi} \end{aligned} \quad (53)$$

$$\begin{aligned} & \left[ -\frac{ES^*}{\Delta^2} + \frac{(ES^*)'}{2\Delta} \right] \phi_{i-1} + \left[ -\frac{EI^*}{\Delta^2} + \frac{(EI^*)'}{2\Delta} \right] u_{i-1}^* + \frac{2ES^*}{\Delta^2} \phi_i + \left( \frac{2EI^*}{\Delta^2} + \kappa GF^* \right) u_i^* \\ & + \left[ -\frac{ES^*}{\Delta^2} - \frac{(ES^*)'}{2\Delta} \right] \phi_{i+1} + \left[ -\frac{EI^*}{\Delta^2} - \frac{(EI^*)'}{2\Delta} \right] u_{i+1}^* = 0 \end{aligned} \quad (54)$$

in which  $\Delta$  = the finite difference mesh;  $v_{i-1}$ ,  $v_i$ ,  $v_{i+1}$ , ... represent displacements at the  $(i-1)$ th,  $i$ th, and  $(i+1)$ th mesh points, respectively, as shown in Figure 4; and  $P_{yi}$  and  $m_{zi}$  = the lateral load and moment, respectively, at the  $i$ th mesh point. In the above equations, the rigidities  $\kappa GA$ ,  $EI$ , ... at the pivotal mesh point  $i$  are taken as the mean value of the rigidities of current prototype tube structures located in the mesh region, in which the mesh region is defined as each half height between the mesh point  $i$  and the adjoin mesh points,  $i-1$  and  $i+1$ , namely from  $(x_i + x_{i-1})/2$  to  $(x_i + x_{i+1})/2$ , as shown in Figure 5. Hence, the stiffness  $k_{(i)}$  at a mesh point  $i$  is evaluated

$$k_{(i)} = \frac{a_{i1}k_{i1} + a_{i2}k_{i2} + \dots + a_{in}k_{in}}{h_{(i)}} \quad (55)$$

in which  $a_{i1}$ ,  $a_{i2}$ , ...,  $a_{in}$  and  $k_{i1}$ ,  $k_{i2}$ , ...,  $k_{in}$  = the effective story heights and story rigidities, located in the mesh region, respectively; and  $h_{(i)}$  = the current mesh region for the pivotal mesh point  $i$ . The first mesh region in the vicinity of the base is defined as region from the base to the mid-height between the mesh points 1 and 2.

Now, the boundary conditions for a doubly-symmetric tube structure are assumed to be fixed at the base and free, except for the shear-lag, at the top. The shear-lag at the top is considered for two cases: free and constrained. Hence, from Eqs. (36) to (38)

$$v = 0 \text{ at } x = 0 \quad (56)$$

$$\phi = 0 \text{ at } x = 0 \quad (57)$$

$$u^* = 0 \text{ at } x = 0 \quad (58)$$

$$v' + \phi = 0 \text{ at } x = L \quad (59)$$

$$ES^* u^{*'} + EI \phi' = 0 \text{ at } x = L \quad (60)$$

$$EI^* u^{*'} + ES \phi' = 0 \text{ at } x = L \text{ ( Shear-lag is free.)} \quad (61a)$$

$$u^* = 0 \text{ at } x = L \text{ ( Shear-lag is constraint. )} \quad (61b)$$

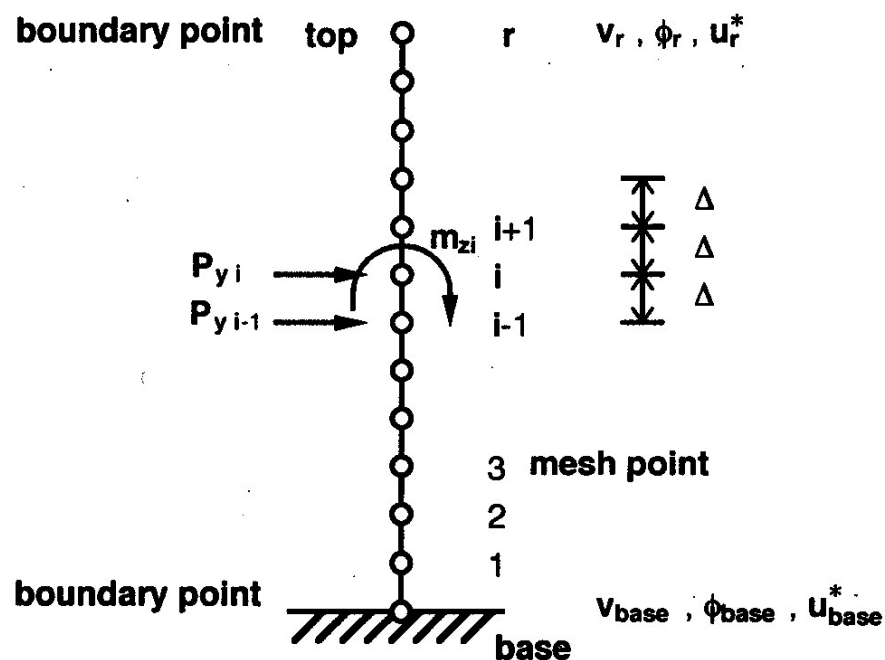


Figure 4. Mesh point in finite difference method [6]

Let us consider the finite difference expression for the boundary conditions (56) - (61). Since tube structures are replaced with an equivalent cantilever in the one-dimensional extended rod theory, the inner points for finite difference method take total numbers  $m$  as shown in Figure 6, in which the mesh point  $m$  locates on the boundary point at  $x=L$ .

Since the number of each boundary condition of the base and top for  $v$ ,  $\phi$  and  $u^*$  is one, respectively, the imaginary number of the boundary mesh in finite differences can be taken one for each displacement component at each boundary.

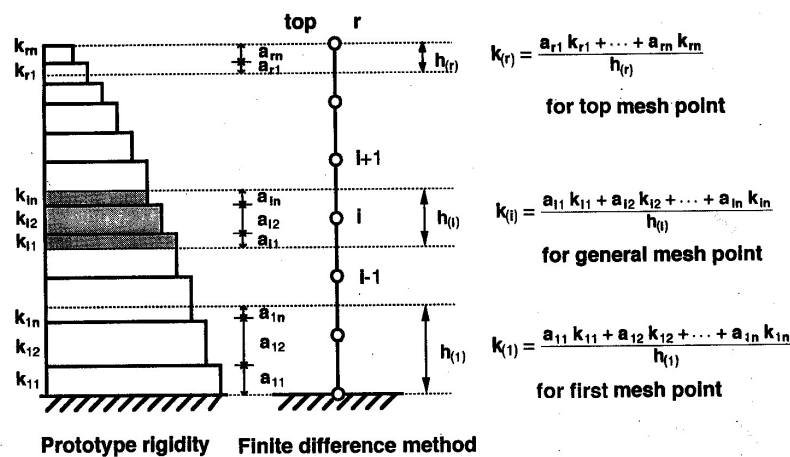


Figure 5. Equivalent rigidity in finite difference method [6]

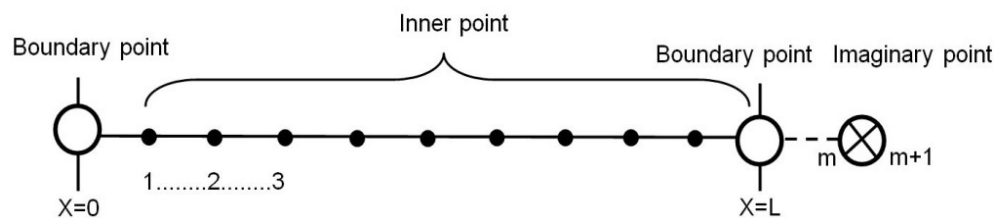


Figure 6. Inner points and imaginary point

The finite differences expressions for the boundary conditions (56)-(58) at the base ( $x=0$ ) are

$$v_{base} = 0 \quad (62)$$

$$\phi_{base} = 0 \quad (63)$$

$$u_{base}^* = 0 \quad (64)$$

in which  $v_{base}$ ,  $\phi_{base}$ , and  $u_{base}^*$  represent quantities at the base.

On the other hand, using central difference method, the finite difference expressions for the boundary conditions (59), (60), and (61a), in case where the shear-lag is free at the top( $x=L$ ), are expressed as

$$[-v_{m-1} + v_{m+1}] \frac{1}{2\Delta} + \phi_m = 0 \quad (65)$$

$$EI[-\phi_{m-1} + \phi_{m+1}] \frac{1}{2\Delta} + ES^*[-u_{m-1}^* + u_{m+1}^*] \frac{1}{2\Delta} = 0 \quad (66)$$

$$ES^*[-\phi_{m-1} + \phi_{m+1}] \frac{1}{2\Delta} + EI^*[-u_{m-1}^* + u_{m+1}^*] \frac{1}{2\Delta} = 0 \quad (67)$$

in which the mesh point  $m$  locates on the boundary point at the free end of  $x=L$ ; the mesh point  $m+1$  is imaginary point adjoining the mesh point  $m$ ; and the mesh point  $m-1$  is inner point adjoining the mesh point  $m$ . Solving the above equations for the variables  $v_{m+1}$ ,  $\phi_{m+1}$ ,  $u_{m+1}^*$  at the imaginary point  $m+1$ , we have

$$v_{m+1} = v_{m-1} - 2\Delta \cdot \phi_m \quad (68)$$

$$\phi_{m+1} = \phi_{m-1} \quad (69)$$

$$u_{m+1}^* = u_{m-1}^* \quad (70)$$

On the other hand, the finite difference expressions for boundary conditions (59), (60), and (61b), in case where the shear-lag is constraint at the top, use the central difference for  $v$  and  $\phi$  but backward difference for  $u^*$ , because  $u_{m+1}^*$  is unsolvable in the use of the central difference.

$$[-v_{m-1} + v_{m+1}] \frac{1}{2\Delta} + \phi_m = 0 \quad (71)$$

$$EI[-\phi_{m-1} + \phi_{m+1}] \frac{1}{2\Delta} + ES^*[-u_{m-1}^* + u_m^*] \frac{1}{\Delta} = 0 \quad (72)$$

$$u_m^* = 0 \quad (73)$$

Solving the above equations for the variables  $v_{m+1}$ ,  $\phi_{m+1}$ ,  $u_m^*$ , we have

$$v_{m+1} = v_{m-1} - 2\Delta \cdot \phi_m \quad (74)$$

$$\phi_{m+1} = \phi_{m-1} + \frac{2ES^*}{EI} u_{m-1}^* \quad (75)$$

$$u_m^* = 0 \quad (76)$$

Static solutions are obtained by solving a system of linear, homogeneous, simultaneous algebraic equation (77) with respect to unknown displacement components at the internal mesh points. In finite difference method the equilibrium equations are formulated on each inner point from 1 to  $m$ .

$$A v = P \quad (77)$$

in which the matrix  $A$  is the total stiffness matrix summed the individual stiffness matrix at each mesh point.  $v$  and  $P$  are the total displacement vector and total external load vector, respectively.

Figure 7 shows stencil of equilibrium equations at a general inner point  $i$ . Figure 8 shows stencil of equilibrium equations at inner point 1 adjoining the base. Figure 9 shows stencil of equilibrium equations at inner point  $i=m$  for the case that the shear-lag is free at the top. Figure 10 shows stencil of equilibrium equations at inner point  $i=m$  for the case that the shear-lag is constrained at the top.

### 3.2. Axial forces of columns

Let us consider the axial forces of columns. The axial stress  $\sigma_x$  of the tube structure is given from Eq. (12) by

$$\sigma_x = E \left[ y \phi'(x, t) + \varphi^*(z) u^*(x, t) \right] \quad (78)$$

Hence, the axial force  $N_i$  in the  $i$ th column with the column's sectional area  $A_i$  is

$$N_i = E \left\{ y \phi' A_i \pm \left[ z - \frac{z^3}{3b_z^2} \right]_{z_1}^{z_2} t_i u^* \right\} \quad (79)$$

for columns in flange surfaces,

$$N_i = E \left[ \frac{1}{2} (y_2 + y_1) A_i \phi' \right] \quad (80)$$

for columns in web surfaces, and



$$N_i = E \left\{ y \phi' A_i \pm \left[ z - \frac{z^3}{3b_z^2} \right]_{z_1}^{z_2} t_i u^{*'} \right\} + E \left[ \frac{1}{2} (y_2^2 - y_1^2) \phi' \right] t_i \quad (81)$$

for corner columns, in which  $y_1$ ,  $y_1$  and  $y_1$ ,  $z_2$  = lower and upper coordinate values of the half between the  $i$ th column and both adjacent columns, respectively, and  $t_i$  = the cross-sectional area  $A_i$  of the  $i$ th column divided by the sum of half spans between the  $i$ th column and the both adjacent columns.

	i-1			i			i+1			P
	$v_{i-1}$	$\phi_{i-1}$	$u_{i-1}^*$	$v_i$	$\phi_i$	$u_i^*$	$v_{i+1}$	$\phi_{i+1}$	$u_{i+1}^*$	
$\delta v$	$-\frac{\kappa GA}{\Delta^2}$ $+\frac{(\kappa GA)'}{2\Delta}$	$+\frac{\kappa GA}{2\Delta}$	0	$+\frac{2\kappa GA}{\Delta^2}$	$-(\kappa GA)'$	0	$-\frac{\kappa GA}{\Delta^2}$ $-\frac{(\kappa GA)'}{2\Delta}$	$-\frac{\kappa GA}{2\Delta}$	0	$= P_{yi}$
$\delta \phi$	$-\frac{\kappa GA}{2\Delta}$	$-\frac{EI}{\Delta^2} + \frac{(EI)'}{2\Delta}$	$-\frac{ES^*}{\Delta^2}$ $+\frac{(ES^*)'}{2\Delta}$	0	$\frac{2EI}{\Delta^2} + \kappa GA$	$\frac{2ES^*}{\Delta^2}$	$\frac{\kappa GA}{2\Delta}$	$-\frac{EI}{\Delta^2}$ $-\frac{(EI)'}{2\Delta}$	$-\frac{ES^*}{\Delta^2}$ $-\frac{(ES^*)'}{2\Delta}$	$= m_i$
$\delta u^*$	0	$-\frac{ES^*}{\Delta^2}$ $+\frac{(ES^*)'}{2\Delta}$	$-\frac{EI^*}{\Delta^2}$ $+\frac{(EI^*)'}{2\Delta}$	0	$\frac{2ES^*}{\Delta^2}$	$\frac{2EI^*}{\Delta^2} + \kappa GF^*$	0	$-\frac{ES^*}{\Delta^2}$ $-\frac{(ES^*)'}{2\Delta}$	$-\frac{EI^*}{\Delta^2}$ $-\frac{(EI^*)'}{2\Delta}$	$= 0$

Figure 7. Stencil of equilibrium equations at inner point  $i$

	i-1 (0)			i (1)			i+1 (2)			P
	$v_{i-1}$	$\phi_{i-1}$	$u_{i-1}^*$	$v_i$	$\phi_i$	$u_i^*$	$v_{i+1}$	$\phi_{i+1}$	$u_{i+1}^*$	
$\delta v$	$\frac{\kappa GA}{\Delta^2}$ $+\frac{(\kappa GA)'}{2\Delta}$	$-\frac{\kappa GA}{2\Delta}$	0	$-\frac{2\kappa GA}{\Delta^2}$	$(\kappa GA)'$	0	$\frac{\kappa GA}{\Delta^2}$ $-\frac{(\kappa GA)'}{2\Delta}$	$\frac{\kappa GA}{2\Delta}$	0	$= P_{yi}$
$\delta \phi$	$-\frac{\kappa GA}{2\Delta}$	$-\frac{EI}{\Delta^2} + \frac{(EI)'}{2\Delta}$	$-\frac{ES^*}{\Delta^2}$ $+\frac{(ES^*)'}{2\Delta}$	0	$\frac{2EI}{\Delta^2} + \kappa GA$	$\frac{2ES^*}{\Delta^2}$	$\frac{\kappa GA}{2\Delta}$	$-\frac{EI}{\Delta^2}$ $-\frac{(EI)'}{2\Delta}$	$-\frac{ES^*}{\Delta^2}$ $-\frac{(ES^*)'}{2\Delta}$	$= m_i$
$\delta u^*$	0	$-\frac{ES^*}{\Delta^2}$ $+\frac{(ES^*)'}{2\Delta}$	$-\frac{EI^*}{\Delta^2}$ $+\frac{(EI^*)'}{2\Delta}$	0	$\frac{2ES^*}{\Delta^2}$	$\frac{2EI^*}{\Delta^2} + \kappa GF^*$	0	$-\frac{ES^*}{\Delta^2}$ $-\frac{(ES^*)'}{2\Delta}$	$-\frac{EI^*}{\Delta^2}$ $-\frac{(EI^*)'}{2\Delta}$	$= 0$

Figure 8. Stencil of equilibrium equations at inner point 1

	i-1 (=m-1)			i (=m)			i+1 (=m+1)			P
	$v_{i-1}$	$\phi_{i-1}$	$u^*_{i-1}$	$v_i$	$\phi_i$	$u^*_i$	$v_{i+1}$	$\phi_{i+1}$	$u^*_{i+1}$	
$\delta v$	$-\frac{\kappa GA}{\Delta^2}$ $+\frac{(\kappa GA)'}{2\Delta}$ $+c17$	$\frac{\kappa GA}{2\Delta}$ $+c18$	0 $+c19$	$\frac{2\kappa GA}{\Delta^2}$	$-(\kappa GA)'$ $-c17(2\Delta)$	0	$-\frac{\kappa GA}{\Delta^2}$ $-\frac{(\kappa GA)'}{2\Delta}$ $c17$	$-\frac{\kappa GA}{2\Delta}$ $c18$	0 $c19$	$= P_{yi}$
$\delta \phi$	$-\frac{\kappa GA}{2\Delta}$ $+c27$	$-\frac{EI}{\Delta^2} + \frac{(EI)'}{2\Delta}$ $+c28$	$-\frac{ES^*}{\Delta^2}$ $+\frac{(ES^*)'}{2\Delta}$ $+c29$	0	$\frac{2EI}{\Delta^2} + \kappa GA$ $-c27(2\Delta)$	$\frac{2ES^*}{\Delta^2}$	$\frac{\kappa GA}{2\Delta}$ $c27$	$-\frac{EI}{\Delta^2}$ $-\frac{(EI)'}{2\Delta}$ $c28$	$-\frac{ES^*}{\Delta^2}$ $-\frac{(ES^*)'}{2\Delta}$ $c29$	$= m_i$
$\delta u^*$	0 $+c37$	$-\frac{ES^*}{\Delta^2}$ $+\frac{(ES^*)'}{2\Delta}$ $+c38$	$-\frac{EI^*}{\Delta^2}$ $+\frac{(EI^*)'}{2\Delta}$ $+c39$	0	$\frac{2ES^*}{\Delta^2}$ $-c37(2\Delta)$	$\frac{2EI^*}{\Delta^2} + \kappa GF^*$	0 $c37$	$-\frac{ES^*}{\Delta^2}$ $-\frac{(ES^*)'}{2\Delta}$ $c38$	$-\frac{EI^*}{\Delta^2}$ $-\frac{(EI^*)'}{2\Delta}$ $c39$	$= 0$

**Figure 9.** Stencil of equilibrium equations at inner point  $i=m$  for the case that the shear-lag is free at the top

	i-1			i			i+1 (F)			P
	$v_{i-1}$	$\phi_{i-1}$	$u^*_{i-1}$	$v_i$	$\phi_i$	$u^*_i$	$v_{i+1}$	$\phi_{i+1}$	$u^*_{i+1}$	
$\delta v$	$-\frac{\kappa GA}{\Delta^2}$ $+\frac{(\kappa GA)'}{2\Delta}$ $+c17$	$\frac{\kappa GA}{2\Delta}$ $+c18$	0 $+c18(\frac{2ES^*}{EI})$	$\frac{2\kappa GA}{\Delta^2}$	$-(\kappa GA)'$ $-c17(2\Delta)$	0	$-\frac{\kappa GA}{\Delta^2}$ $-\frac{(\kappa GA)'}{2\Delta}$ $c17$	$-\frac{\kappa GA}{2\Delta}$ $c18$	0 $c19$	$= P_{yi}$
$\delta \phi$	$-\frac{\kappa GA}{2\Delta}$ $+c27$	$-\frac{EI}{\Delta^2} + \frac{(EI)'}{2\Delta}$ $+c28$	$-\frac{ES^*}{\Delta^2} + \frac{(ES^*)'}{2\Delta}$ $+c28(\frac{2ES^*}{EI})$	0	$\frac{2EI}{\Delta^2} + \kappa GA$ $-c27(2\Delta)$	$\frac{2ES^*}{\Delta^2}$	$\frac{\kappa GA}{2\Delta}$ $c27$	$-\frac{EI}{\Delta^2}$ $-\frac{(EI)'}{2\Delta}$ $c28$	$-\frac{ES^*}{\Delta^2}$ $-\frac{(ES^*)'}{2\Delta}$ $c29$	$= m_i$
$\delta u^*$	0 $+c37$	$-\frac{ES^*}{\Delta^2}$ $+\frac{(ES^*)'}{2\Delta}$ $+c38$	$-\frac{EI^*}{\Delta^2}$ $+\frac{(EI^*)'}{2\Delta}$ $+c38(\frac{2ES^*}{EI})$	0	$\frac{2ES^*}{\Delta^2}$ $-c37(2\Delta)$	$\frac{2EI^*}{\Delta^2} + \kappa GF^*$	0 $c37$	$-\frac{ES^*}{\Delta^2}$ $-\frac{(ES^*)'}{2\Delta}$ $c38$	$-\frac{EI^*}{\Delta^2}$ $-\frac{(EI^*)'}{2\Delta}$ $c39$	$= 0$

**Figure 10.** Stencil of equilibrium equations at inner point  $i=m$  for the case that the shear-lag is constrained at the top

#### 4. Free transverse vibrations by finite difference method

Consider free transverse vibrations of the current doubly-symmetric tube structures by means of the finite difference method. Now,  $v(x, t)$ ,  $\phi(x, t)$ , and  $u^*(x, t)$  are expressed as

$$v(x, t)=\bar{v}(x, t)\exp\{i\omega t\} \tag{82}$$

$$\phi(x, t)=\bar{\phi}(x, t)\exp\{i\omega t\} \tag{83}$$

$$u^*(x, t)=\bar{u}^*(x, t)\exp\{i\omega t\} \tag{84}$$

Substituting the above equations into the equations of motion for the free transverse vibration obtained from Eqs. (32)-(39), the equations for free vibrations become

$$\delta v:\omega^2 m\bar{v} + [\kappa GA(\bar{v}' + \bar{\phi})]'=0 \tag{85}$$

$$\delta \phi:\omega^2 \rho I \bar{\phi} + \omega^2 \rho S^* \bar{u}^* + (EI \bar{\phi})' - \kappa GA(\bar{v}' + \bar{\phi}) + (ES^* \bar{u}^*)' = 0 \tag{86}$$

$$\delta u^*:\omega^2 \rho S^* \bar{\phi} + \omega^2 \rho I^* \bar{u}^* + (EI^* \bar{u}^*)' + (ES^* \bar{\phi})' - \kappa GF^* \bar{u}^* = 0 \tag{87}$$

The finite difference expressions of the above equations reduce to eigenvalue problem for  $\bar{v}$  ,  $\bar{\phi}$  , and  $\bar{u}^*$  .

$$[A-\omega^2 B] v=0 \tag{88}$$

Here the matrix **A** is the total stiffness matrix as given in Eq. (78). On the other hand, the matrix **B** is total mass matrix which is the sum of individual mass matrix. The individual mass matrix at the *i*th mesh point is given in Figure 11. The *i*th natural frequencies  $\omega_i$  can be obtained from the *i*th eigenvalue.

i		
$v_i$	$\phi_i$	$u_i^*$
$-\rho A$	0	0
0	$-\rho I$	$-\rho S^*$
0	$-\rho S^*$	$-\rho I^*$

**Figure 11.** Individual mass matrix at mesh point *i*

## 5. Forced transverse vibrations by finite difference method

Forced lateral vibration of current tube structures may be obtained easily by means of modal analysis for elastic behavior subject to earthquake motion. Applying the finite difference method into Eq. (32), the equation of motion of current tube structures with distributed properties may be changed to discrete structure with degrees of freedom three times the total number of mesh points because each mesh point has three freedoms for the displacement components. Hence, Eq. (32) for current tube structure, subjected to earthquake acceleration  $\ddot{v}_0$  at the base may be written in the matrix form as

$$[M]\{\ddot{v}\} + [c_v]\{\dot{v}\} - [\kappa GA(v' + \phi)'] = -[M]\{1\}\ddot{v}_0 \quad (89)$$

in which  $[M]$  = mass matrix;  $[c_v]$  = the damping coefficient matrix; and  $\{\ddot{v}\}$ ,  $\{\dot{v}\}$ , and  $\{v\}$  are the relative acceleration vector, the relative velocity vector and relative displacement vector, respectively, measured from the base.  $\{1\}$  = unit vector. It is assumed that the dynamic deflection vector  $\{v\}$  and the rotational angle vector  $\{\phi\}$  may be written as

$$\{v\} = \sum_{j=1}^n \beta_j \{v\}_j q_j(t) \quad (90)$$

$$\{\phi\} = \sum_{j=1}^n \beta_j \{\phi\}_j q_j(t) \quad (91)$$

in which  $\beta_j$  = the  $j$ -th participation coefficient;  $\{v\}_j$  and  $\{\phi\}_j$  = the  $j$ -th eigenfunctions for  $v$  and  $\phi$ , respectively;  $q_j(t)$  = the  $j$ -th dynamic response depending on time  $t$ ; and  $n$  = the total number of degrees of freedom taken into consideration here. Substituting Eqs. (90) and (91) into Eq. (89) and multiplying the reduced equation by  $\{v\}_i^T$ , we have

$$\begin{aligned} & \{v\}_i^T [M] \{v\}_i \ddot{q}_i(t) + \{v\}_i^T [c_v] \{v\}_i \dot{q}_i(t) - \\ & [\{v\}_i^T (\kappa GA) \{v\}_i q_i + \{v\}_i^T (\kappa GA)' \{v\}_i q_i] \beta_i = -\{v\}_i^T [M] \{1\} \ddot{v}_0 \end{aligned} \quad (92)$$

Now, Eq. (86) may be rewritten as

$$\omega^2 [M] \{v\}_i - [\kappa GA(\{v\}_i' + \{\phi\}_i')] = 0 \quad (93)$$

Multiplying the above equation by  $\{v\}_i^T$  and substituting the reduced equation into Eq. (93), we have

$$\{v\}_i^T [M] \{v\}_i \ddot{q}_i(t) + \{v\}_i^T [c] \{v\}_i \dot{q}_i(t) + \beta_i \omega^2 \{v\}_i^T [M] \{v\}_i q_i = -\{v\}_i^T [M] \{1\} \ddot{v}_0 \quad (94)$$

Here, the damping coefficient matrix  $[c_v]$  and the participation coefficients  $\beta_i$  are assumed to satisfy the following expressions:

$$\frac{\{v\}_i^T [c_v] \{v_i\}}{\{v\}_i^T [M] \{v_i\}} = 2h_i \omega_i \quad (95)$$

$$\beta_i = \frac{\{v\}_i^T [M] \{1\}}{\{v\}_i^T [M] \{v_i\}} \quad (96)$$

in which  $h_i$  is the  $i$ th damping constant. Thus, Eq. (94) may be reduced to

$$\ddot{q}_i(t) + 2h_i \omega_i \dot{q}_i(t) + \omega_i^2 q_i(t) = -\ddot{v}_0 \quad (97)$$

The general solution of Eq. (98) is

$$q_i(t) = \exp(-h_i \omega_i t) (C_1 \sin \omega_{Di} t + C_2 \cos \omega_{Di} t) - \frac{1}{\omega_{Di}} \int_0^t \exp[-h_i \omega_i (t - \tau)] \sin \omega_{Di} (t - \tau) \ddot{v}_0 d\tau \quad (98)$$

in which  $\omega_{Di} = \omega_i \sqrt{1 - h_i^2}$  and  $C_1$  and  $C_2$  are constants determined from the initial conditions. The Duhamel integral in Eq. (98) may be calculated approximately by means of Paz [19] or Takabatake [2].

## 6. Numerical results by finite difference method

### 6.1. Numerical models

Numerical models for examining the simplified analysis proposed here are shown in Figure 12. These numerical models are determined to find out the following effects: (1) the effect of the aspect ratio of the outer and inner tubes; (2) the effect of omitting the corners; and (3) the effect of bracing. **Model T1** is a doubly symmetric single frame-tube prepared for comparison with the numerical results of the doubly symmetric frame-double-tube. **T7** and **T8** are made up steel reinforced concrete frame-tubes, and the other models are steel frame-tubes. The total number of stories is 30. The difference between models **T2** to **T5** concerns the number of story and span attached bracing. The members of the single and double tubes are shown in Figures 13 and 14.

In the numerical computation, the following assumptions are made:

1. the static lateral force is a triangularly distributed load, as shown in Figures 13 and 14;

2. the dynamic loads are taken from El Centro 1940 NS, Taft 1952 EW, and Hachinohe 1968 NS, in which each maximum acceleration is  $200 \text{ m/s}^2$ ;
3. the damping ratio for the first mode of the frame-tubes is  $h_1 = 0.02$ , and the higher damping ratio for the  $n$ -th mode is  $h_1 = h_1 \omega_n / \omega_1$ ;
4. the weight of each floor is  $9.807 \text{ kN/m}^2$  and the mass of the frame-tube is considered to be only floor's weight;
5. in the modal analysis, the number of modes for the participation coefficients is taken five into consideration as five.


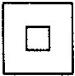
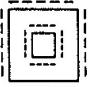


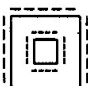


MODEL (1)	PLAN (2)	BRACING (3)	CONSTRUCTION (4)
T 1			STEEL
T 2			STEEL
T 3		15, 16 STORY	STEEL
T 4		9, 10 STORY	STEEL
T 5		15, 16 STORY	STEEL
T 6		15, 16, 29, 30 STORY	STEEL
T 7			STEEL REINFORCED CONCRETE
T 8			STEEL REINFORCED CONCRETE

Figure 12. Numerical models [6]

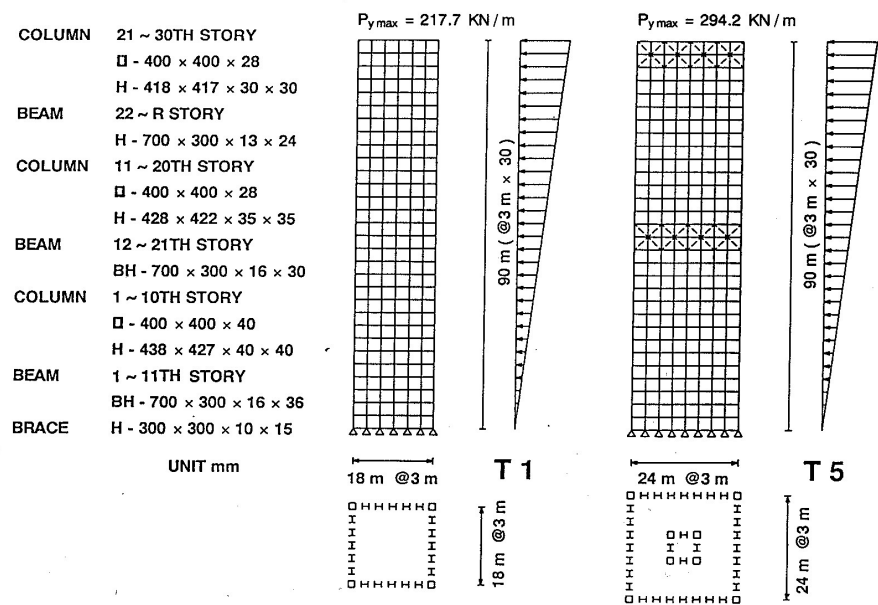


Figure 13. Member of numerical models T1 and T5 [6]

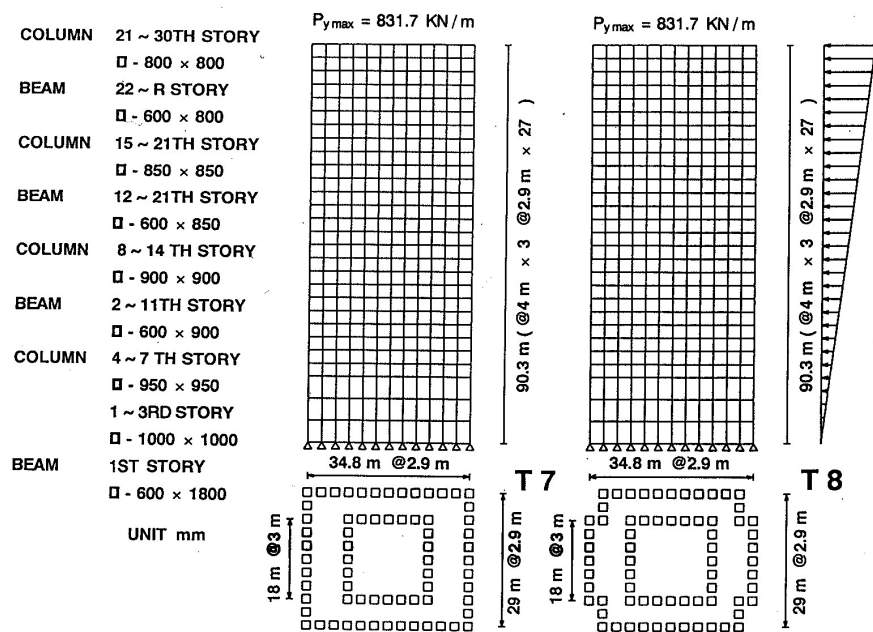


Figure 14. Member of numerical models T7 and T8 [6]

6.2. Static numerical results

First, the static numerical results are stated. Tables 1 and 2 show the maximum values of the static lateral displacements and shear-lags, calculated from the present theory, NASTRAN and DEMOS, in which a discrepancy between results obtained from NASTRAN and DE-

MOS is negligible, in practice. The ratios are those of the values obtained from the present theory to the corresponding values from the three-dimensional frame analysis using NASTRAN and DEMOS. The distributions of the static lateral displacements are shown in Figure 15. These numerical results show the simplified analysis is in good agreement, in practice, with the results of three-dimensional frame analysis using NASTRAN and DEMOS. Since the shear-lag is far smaller than the transverse deflections, as shown in Table 2 the discrepancy in shear-lag is negligible in practice.

Maximum static lateral deflection (m)			
Model (1)	Present theory (2)	Frame analysis (3)	Ratio(2)/(3) (4)
T1	0.441	0.430	1.026
T2	0.327	0.343	0.953
T3	0.307	0.318	0.965
T4	0.299	0.319	0.937
T5	0.312	0.330	0.945
T6	0.329	0.311	1.058
T7	0.151	0.158	0.956
T8	0.157	0.166	0.946

**Table 1.** Maximum values of static lateral deflections [6]

Maximum shear-lag (m)			
Model (1)	Present theory (2)	Frame analysis (3)	Ratio(2)/(3) (4)
T1	0.0145	0.0079	1.835
T2	0.0149	0.0085	1.753
T7	0.0090	0.0052	1.731
T8	0.0103	0.0028	3.679

**Table 2.** Maximum values of static shear-lags [6]

Figure 16 shows the distribution of axial forces of model T2. A discrepancy between the results obtained from the proposed theory and those from three-dimensional frame analysis is found. However, this discrepancy is within 10 % and is also allowable for practical use because the axial forces in tube structures are designed from the axial forces on the flange surfaces, being always larger than those on the web surfaces.



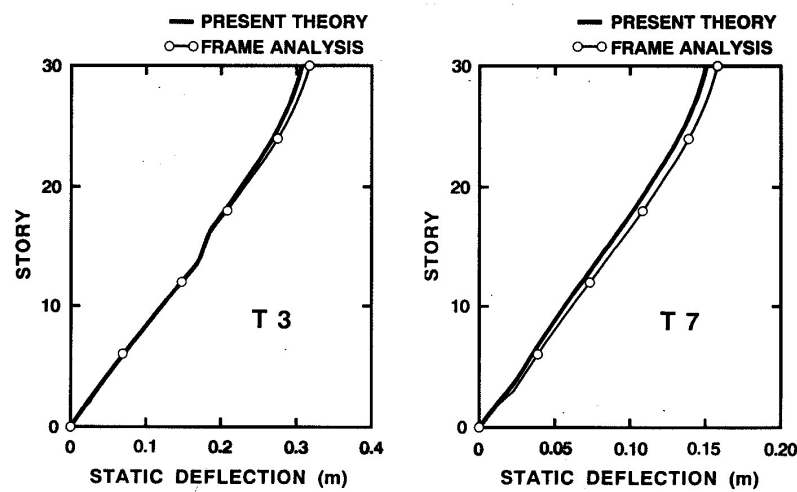


Figure 15. Distribution of static lateral deflection [6]

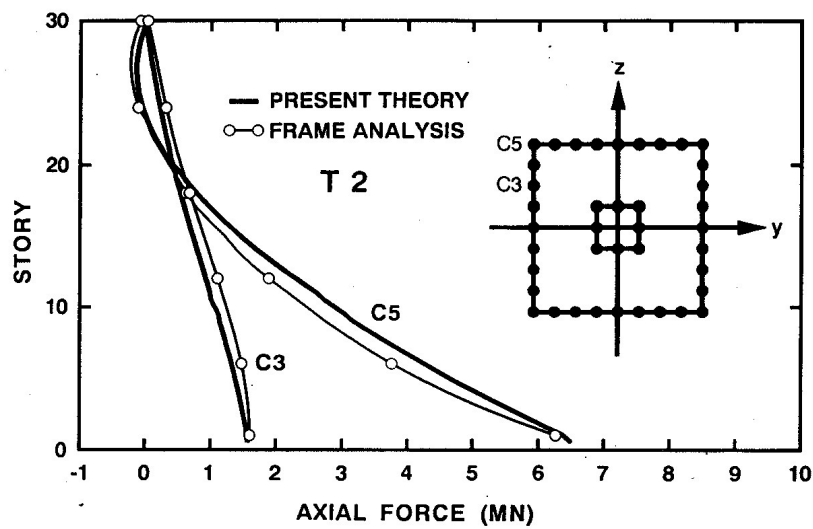


Figure 16. Axial force [6]

		Natural frequency (rad/s)				
Model	Analytical	First	Second	Third	Fourth	Fifth
(1)	methods	(3)	(4)	(5)	(6)	(7)
(2)						
T1	Present theory	1.998	6.077	10.942	15.759	20.397
	Frame analysis	2.062	6.211	11.048	15.907	20.648
	Ratio	0.969	0.978	0.990	0.991	0.988
T2	Present theory	2.080	6.255	11.150	15.977	20.614

Natural frequency (rad/s)						
Model (1)	Analytical methods (2)	First (3)	Second (4)	Third (5)	Fourth (6)	Fifth (7)
T3	Frame analysis	2.058	6.223	11.076	16.020	20.826
	Ratio	1.011	1.005	1.007	0.997	0.990
	Present theory	2.137	6.197	11.694	15.924	21.740
	Frame analysis	2.138	6.290	11.687	16.198	22.062
	Ratio	1.000	0.985	1.001	0.983	0.985
T4	Present theory	2.192	6.186	11.112	16.805	21.334
	Frame analysis	2.152	6.296	11.224	16.813	21.756
	Ratio	1.019	0.983	0.990	1.000	0.981
T5	Present theory	2.126	6.266	11.559	16.073	21.390
	Frame analysis	2.100	6.260	11.464	16.136	21.636
	Ratio	1.012	1.001	1.008	0.996	0.989
T6	Present theory	2.055	6.045	11.631	16.053	22.019
	Frame analysis	2.147	6.369	11.848	16.662	22.610
	Ratio	0.957	0.949	0.982	0.963	0.974
T7	Present theory	3.458	9.920	17.924	25.863	32.626
	Frame analysis	3.462	10.037	17.983	26.246	34.675
	Ratio	0.999	0.988	0.997	0.985	0.941
T8	Present theory	3.401	9.811	17.825	25.786	32.696
	Frame analysis	3.382	9.856	17.729	26.028	34.561
	Ratio	1.006	0.995	1.005	0.991	0.946

**Table 3.** Natural frequencies [6]. Note. Ratio = present theory/frame analysis

### 6.3. Free vibration results

Secondly, consider the natural frequencies. Table 3 shows the natural frequencies of the above-mentioned numerical models. It follows that, in practical use, the simplified analysis gives in excellent agreement with the results obtained from the three-dimensional frame analysis using NASTRAN and DEMOS. Since the transverse stiffness of the bracing is far larger than for frames, the transverse stiffness of current frame-tube with braces varies discontinuously, particularly at the part attached to the bracing. However, such discontinuous and local variation due to bracing can be expressed by the present theory.

### 6.4. Dynamic results

Thirdly, let us present dynamic results. The maximum values of dynamic deflections, story shears, and overturning moments are shown in Tables 4-6, respectively. Figure 17 shows the distribution of the maximum dynamic deflections and of the maximum story shear forces of model **T7** for El Centro 1949 NS. Figure 18 indicates the distribution of the absolute accelera-

tions and of the maximum overturning moments for model **T7**. Thus, the proposed approximate theory is in good agreement with the results of the three-dimensional frame analysis using NASTRAN and DEMOS in practice. These excellent agreements may be estimated from participation functions as shown in Figure 19. The present one-dimensional extended rod theory used the finite difference method can always express discontinuous and local behavior caused by the part attached to the bracing.

Maximum dynamic lateral deflection (m)					
Model (1)	Earthquake type (2)		Present theory (3)	Frame analysis (4)	Ratio(3)/(4) (5)
T1	El Centro	NS	0.263	0.293	0.898
	Hachinohe	NS	0.453	0.411	1.102
	Taft	EW	0.213	0.208	1.024
T2	El Centro	NS	0.311	0.291	1.069
	Hachinohe	NS	0.420	0.419	1.002
	Taft	EW	0.212	0.213	0.995
T3	El Centro	NS	0.327	0.329	0.994
	Hachinohe	NS	0.460	0.465	0.989
	Taft	EW	0.205	0.206	0.995
T4	El Centro	NS	0.318	0.324	0.981
	Hachinohe	NS	0.515	0.469	1.098
	Taft	EW	0.196	0.201	0.975
T5	El Centro	NS	0.327	0.315	1.038
	Hachinohe	NS	0.454	0.429	1.058
	Taft	EW	0.207	0.212	0.976
T6	El Centro	NS	0.297	0.321	0.925
	Hachinohe	NS	0.424	0.437	0.970
	Taft	EW	0.211	0.207	1.019
T7	El Centro	NS	0.155	0.150	1.033
	Hachinohe	NS	0.202	0.195	1.036
	Taft	EW	0.221	0.215	1.028
T8	El Centro	NS	0.158	0.154	1.026
	Hachinohe	NS	0.232	0.235	0.987
	Taft	EW	0.219	0.210	1.043

**Table 4.** Maximum dynamic lateral deflections [6]

The above-mentioned numerical computations are obtained from that the total number of mesh points, including the top, is 60. Figure 20 shows the convergence characteristics of the static and dynamic responses for model **T7**, due to the number of mesh points. The conver-

gence is obtained by the number of mesh points, being equal to the number of stories of the tube structures.

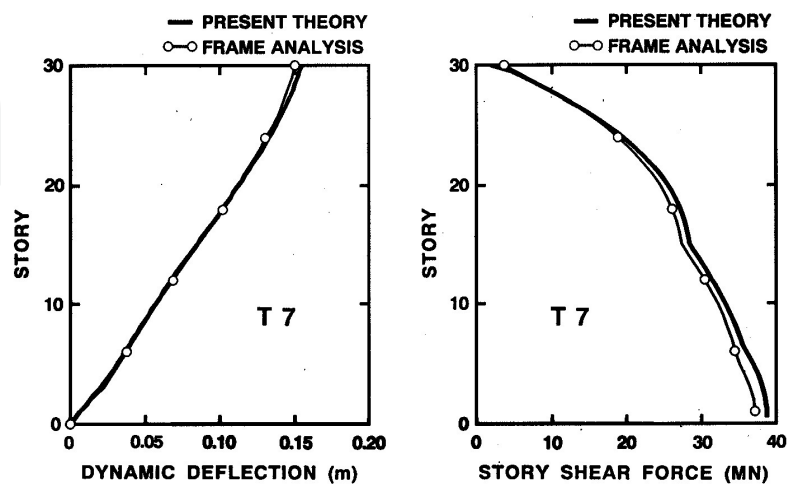
Maximum story shear (kN)					
Model (1)	Earthquake type (2)		Present theory (3)	Frame analysis (4)	Ratio(3)/(4) (5)
T1	El Centro	NS	5482	6659	0.823
	Hachinohe	NS	12494	10003	1.249
	Taft	EW	4972	4835	1.028
T2	El Centro	NS	11464	11082	1.035
	Hachinohe	NS	17260	17309	0.997
	Taft	EW	8414	8071	1.043
T3	El Centro	NS	12239	11768	1.040
	Hachinohe	NS	18937	19378	0.977
	Taft	EW	9248	9012	1.026
T4	El Centro	NS	14749	12258	1.203
	Hachinohe	NS	27498	21084	1.304
	Taft	EW	9316	9307	1.001
T5	El Centro	NS	11484	11180	1.027
	Hachinohe	NS	18172	17515	1.038
	Taft	EW	8865	8659	1.024
T6	El Centro	NS	11562	12160	0.951
	Hachinohe	NS	17632	20270	0.870
	Taft	EW	9807	9150	1.072
T7	El Centro	NS	38746	37167	1.042
	Hachinohe	NS	56153	53642	1.047
	Taft	EW	56731	54819	1.035
T8	El Centro	NS	41306	40109	1.030
	Hachinohe	NS	59595	57957	1.028
	Taft	EW	49004	44718	1.096

Table 5. Maximum story shears [6]

Maximum overturning moment (MN m)					
Model (1)	Earthquake type (2)		Present theory (3)	Frame analysis (4)	Ratio(3)/(4) (5)
T1	El Centro	NS	3.233	3.991	0.810
	Hachinohe	NS	6.099	5.599	1.089
	Taft	EW	2.731	2.863	0.954

Maximum overturning moment (MN m)					
Model (1)	Earthquake type (2)		Present theory (3)	Frame analysis (4)	Ratio(3)/(4) (5)
T2	El Centro	NS	7.118	6.531	1.090
	Hachinohe	NS	9.829	9.413	1.044
	Taft	EW	4.928	4.849	1.016
T3	El Centro	NS	8.090	7.972	1.015
	Hachinohe	NS	11.277	11.122	1.014
	Taft	EW	5.129	5.070	1.012
T4	El Centro	NS	8.140	7.727	1.053
	Hachinohe	NS	13.827	10.983	1.259
	Taft	EW	4.984	5.021	0.993
T5	El Centro	NS	7.879	7.315	1.077
	Hachinohe	NS	10.778	10.250	1.052
	Taft	EW	5.053	5.007	1.009
T6	El Centro	NS	6.566	8.070	0.814
	Hachinohe	NS	9.593	11.431	0.839
	Taft	EW	4.968	5.091	0.976
T7	El Centro	NS	22.148	21.574	1.027
	Hachinohe	NS	29.914	28.929	1.034
	Taft	EW	32.186	31.675	1.016
T8	El Centro	NS	21.662	21.659	1.000
	Hachinohe	NS	32.693	33.462	0.977
	Taft	EW	28.779	28.246	1.019

**Table 6.** Maximum overturning moments [6]



**Figure 17.** Distribution of dynamic lateral deflection and story shear force [6]

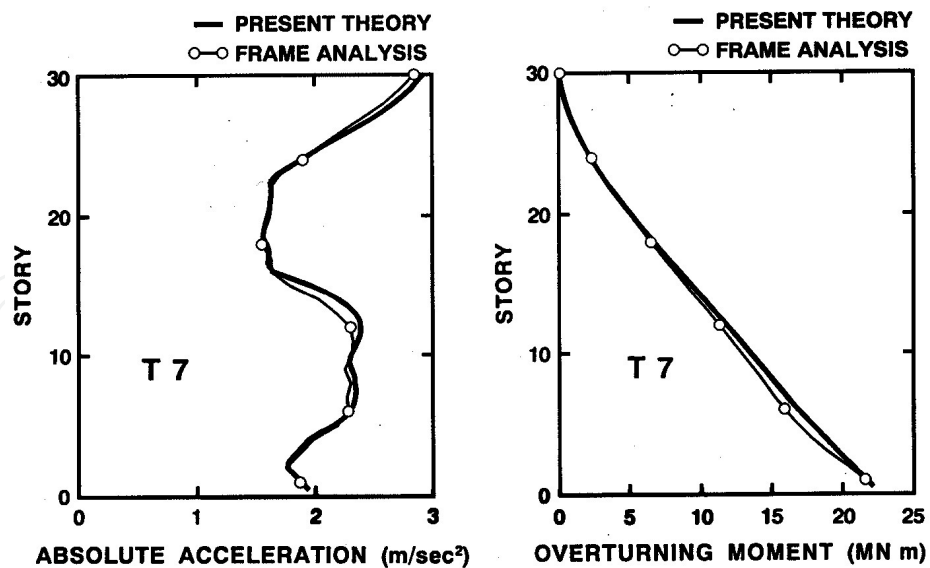


Figure 18. Distribution of absolute acceleration and overturning moment [6]

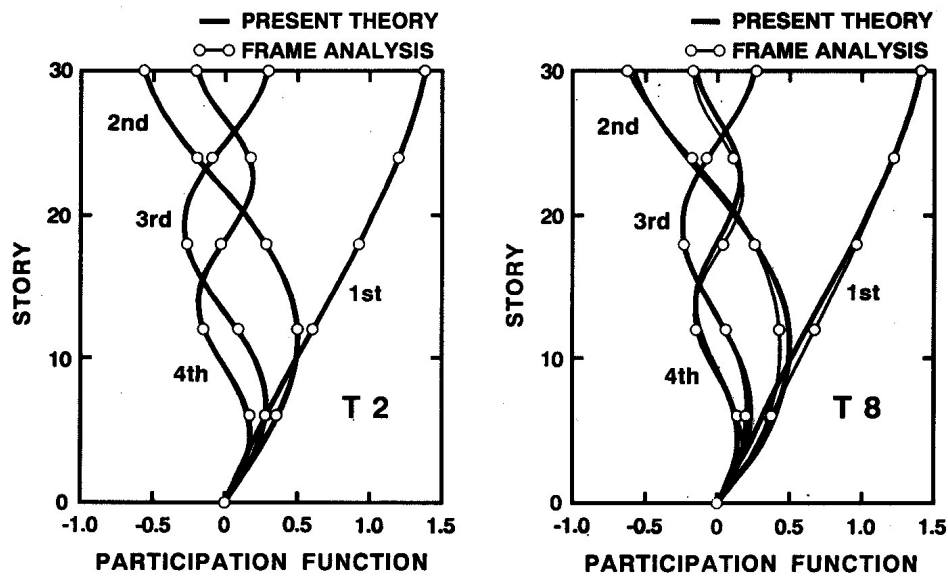


Figure 19. Participation functions [6]

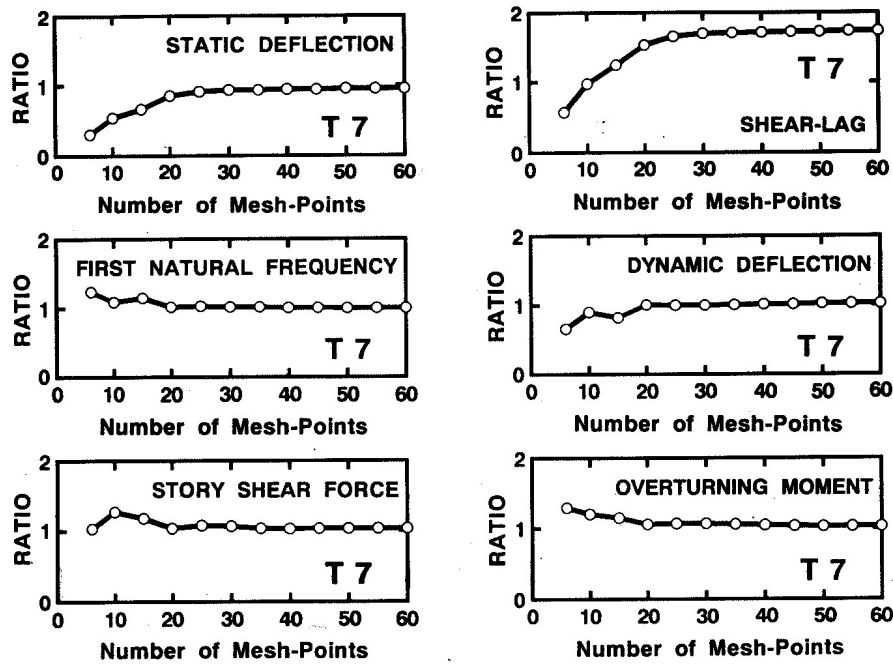


Figure 20. Convergence characteristics [6]

## 7. Natural frequencies by approximate method

### 7.1. Simplification of governing equation

In the structural design of high-rise buildings, structure designers want to grasp simply the natural frequencies in the preliminary design stages. Takabatake [3] presented a general and simple analytical method for natural frequencies to meet the above demands. This section explains about this simple but accurate analytical method.

The one-dimensional extended rod theory for the transverse motion takes the coupled equations concerning  $v$ ,  $\phi$ , and  $u^*$ , as given in Eqs. (32) to (34). Now consider the equation of motion expressed in terms with the lateral deflection. Neglecting the differential term of the transverse shear stiffness,  $\kappa GA$ , in Eq. (32), the differential of rotational angle with respect to  $x$  may be written as

$$\phi = -v'' + \frac{1}{\kappa GA}(-P_y + \rho A \ddot{v} + c_v \dot{v}) \quad (99)$$

From (33) and (34),  $u^*$  becomes

$$u^* = \frac{1}{\kappa G F^*} \frac{I^*}{S^*} [\rho \hat{I} \ddot{\phi} - E \hat{I} \phi'' + \kappa GA(v' + \phi)] \quad (100)$$

in which  $\hat{I}$  is defined as

$$\hat{I} = I \left[ 1 - \frac{(S^*)^2}{II^*} \right] \quad (101)$$

Differentiating Eq. (33) with respect to  $x$  and substituting Eqs. (32), (99), and (100) into the result, the equation of motion expressed in terms with the transverse deflection may be written as

$$\begin{aligned} EI v'''' + \rho A \ddot{v} + c_v \dot{v} - P_y - \rho I \ddot{v}'' - \frac{EI}{\kappa GA} (-P_y'' + \rho A \ddot{v}'' + c_v \dot{v}'') - \frac{EI^*}{\kappa GF^*} (-P_y'' + \rho A \ddot{v}'' + c_v \dot{v}'') \\ + \left( \frac{\rho I}{\kappa GA} + \frac{\rho I^*}{\kappa GF^*} \right) (-P_y + \rho A \ddot{v} + c_v \dot{v})' + \frac{\rho I^*}{\kappa GF^*} E \hat{I} \ddot{v}'''' - \frac{\rho I^*}{\kappa GF^*} \frac{E \hat{I}}{\kappa GA} (-P_y'' + \rho A \ddot{v}'' + c_v \dot{v}'')' \\ + \frac{\rho I^*}{\kappa GF^*} \frac{\rho \hat{I}}{\kappa GA} (-P_y + \rho A \ddot{v} + c_v \dot{v})' - \frac{\rho I^*}{\kappa GF^*} \rho \hat{I} \ddot{v}'' + \frac{EI^*}{\kappa GF^*} \rho \hat{I} \ddot{v}'''' \\ - \frac{EI^*}{\kappa GF^*} \frac{\rho \hat{I}}{\kappa GA} (-P_y + \rho A \ddot{v} + c_v \dot{v}) \\ - \frac{EI^*}{\kappa GF^*} E \hat{I} v'''' + \frac{EI^*}{\kappa GF^*} \frac{E \hat{I}}{\kappa GA} (-P_y + \rho A \ddot{v} + c_v \dot{v})'''' = 0 \end{aligned} \quad (102)$$

Eq. (102) is a sixth-order partial differential equation with variable coefficients with respect to  $x$ . In order to simplify the future development, considering only bending, transverse shear deformation, shear lag, inertia, and rotatory inertia terms in Eq. (102), a simplified governing equation is given

$$EI v'''' + \rho A \ddot{v} + c_v \dot{v} - P_y - \rho I \ddot{v}'' - \frac{EI}{\kappa GA} \left( 1 + \frac{\kappa G A I^*}{I \kappa GF^*} \right) (-P_y'' + \rho A \ddot{v}'' + c_v \dot{v}'') = 0 \quad (103)$$

The equation neglecting the underlined term in Eq. (103) reduces to the equation of motion of Timoshenko beam theory, for example, Eq. (9.49) Craig [20]. Since Eq. (103) is very simple equation, the free transverse vibration analysis is developed by means of Eq. (103). To simplify the future expression, the following notation is introduced

$$(\underline{\kappa GA}) = \kappa GA \frac{1}{1 + \frac{\kappa G A I^*}{\kappa G F^* I}} \quad (104)$$

Hence, Eq. (104) may be rewritten



$$EI v'''' + \rho A \ddot{v} + c_v \dot{v} - P_y - \rho I \ddot{v}'' - \frac{EI}{(\kappa GA)} (-P_y'' + \rho A \ddot{v}'' + c_v \dot{v}'') = 0 \quad (105)$$

The aforementioned equation suggests that in the simplified equation the transverse shear stiffness  $\kappa GA$  must be replaced with the modified transverse shear stiffness  $\underline{(\kappa GA)}$ .

## 7.2. Undamped free transverse vibrations

Let us consider undamped free transverse vibration of high-rise buildings. The equation for undamped free transverse vibrations is written from Eq. (105) as

$$v'''' - \frac{\rho A}{EI} \left[ \frac{\rho I}{\rho A} + \frac{EI}{(\kappa GA)} \right] \ddot{v}'' + \frac{\rho A}{EI} \ddot{v} = 0 \quad (106)$$

Using the separation method of variables,  $v(x, t)$  is expressed as

$$v(x, t) = \Phi(x) e^{i\omega t} \quad (107)$$

Substituting the above equation into Eq. (106), the equation for free vibrations becomes

$$\Phi + b \Phi'''' + c \Phi = 0 \quad (108)$$

in which the coefficients,  $b$  and  $c$ , are defined as

$$b = \frac{(kL)^4}{L^2} \left( \frac{1}{\hat{\lambda}_0} \right)^2 \quad (109)$$

$$c = -k^4 \quad (110)$$

in which  $k^4$  and  $\hat{\lambda}_0$  are defined as

$$k^4 = \frac{\rho A}{EI} \omega^2 \quad (111)$$

$$\left(\frac{1}{\hat{\lambda}_0}\right)^2 = \left(\frac{1}{\lambda_0^*}\right)^2 + \left(\frac{1}{\lambda_0}\right)^2 \quad (112)$$

in which  $\lambda_0^*$  and  $\lambda_0$  are defined as

$$\lambda_0^* = L \sqrt{\frac{\rho A}{\rho I}} \quad (113)$$

$$\lambda_0 = L \sqrt{\frac{(\kappa G A)}{E I}} \quad (114)$$

$\lambda_0^*$  and  $\lambda_0$  are pseudo slenderness ratios of the tube structures, depending on the bending stiffness and the transverse shear stiffness, respectively. Since for a variable tube structure the coefficients,  $b$  and  $c$ , are variable with respect to  $x$ , it is difficult to solve analytically Eq. (108). So, first we consider a uniform tube structure where these coefficients become constant. The solution for a variable tube structure will be presented by means of the Galerkin method.

Thus, since for a uniform tube structure Eq. (108) becomes a fourth-order differential equation with constant coefficients, the general solution is

$$\Phi = C_1 \cos \lambda_1 x + C_2 \sin \lambda_1 x + C_3 \sin h \lambda_2 x + C_4 \cosh \lambda_2 x \quad (115)$$

in which  $C_1$  to  $C_4$  are integral constants and  $\lambda_1$  and  $\lambda_2$  are defined as

$$\lambda_1 = \frac{(kL)^2}{L} \alpha_1^* \quad (116)$$

$$\lambda_2 = \frac{(kL)^2}{L} \alpha_2^* \quad (117)$$

in which  $\alpha_1^*$  and  $\alpha_2^*$  are

$$\alpha_1^* = \frac{1}{\hat{\lambda}_0} \sqrt{\frac{1+\alpha}{2}} \quad (118)$$

$$\alpha_2^* = \frac{1}{\hat{\lambda}_0} \sqrt{\frac{-1 + \alpha}{2}} \quad (119)$$

in which

$$\alpha = \sqrt{1 + \frac{4}{(kL)^4 \left(\frac{1}{\hat{\lambda}_0}\right)^4}} \quad (120)$$

Meanwhile,  $\phi'$  for the free transverse vibration is from Eq. (99)

$$\phi' = -v'' + \frac{\rho A}{(\kappa GA)} \ddot{v} \quad (121)$$

in which  $\kappa GA$  is replaced with  $(\kappa GA)$ . The substitution of Eqs. (108) and (111) into the aforementioned equation yields

$$\phi'(x, t) = - \left[ \Phi(x) + k^4 \frac{EI}{(\kappa GA)} \Phi(x) \right] e^{i\omega t} \quad (122)$$

The integration of the aforementioned equation becomes

$$\phi(x, t) = - \left[ \Phi'(x) + k^4 \frac{EI}{(\kappa GA)} \int \Phi(x) dx \right] e^{i\omega t} \quad (123)$$

The boundary conditions for the current tube structures are assumed to be constrained for all deformations at the base and free for bending moment, transverse shear and shear-lag at the top. Hence the boundary conditions are rewritten from Eqs. (35) to (38) as

$$v = 0 \quad \text{at } x = 0 \quad (124)$$

$$\phi = 0 \quad \text{at } x = 0 \quad (125)$$

$$u^* = 0 \quad \text{at } x = 0 \quad (126)$$

$$v' + \phi = 0 \text{ at } x = L \quad (127)$$

$$E S * u^{*'} + E I \phi' = 0 \text{ at } x = L \quad (128)$$

$$EI * u^{*'} + ES * \phi' = 0 \text{ at } x = L \quad (129)$$

Eqs. (128) and (129) reduce to

$$\phi' = 0 \text{ at } x = L \quad (130a)$$

$$u^{*'} = 0 \text{ at } x = L \quad (130b)$$

Hence the boundary conditions for current problem become as Eqs. (124), (125), (127), and (130a). Using Eq. (107), these boundary conditions are rewritten as

$$\Phi = 0 \text{ at } x = 0 \quad (131)$$

$$\Phi'(x) + k^4 \frac{EI}{(\kappa GA)} \int \Phi(x) dx = 0 \text{ at } x = 0 \quad (132)$$

$$\int \Phi(x) dx = 0 \text{ at } x = L \quad (133)$$

$$\Phi''(x) + k^4 \frac{EI}{(\kappa GA)} \Phi(x) = 0 \text{ at } x = L \quad (134)$$

Substituting Eq. (115) into the aforementioned boundary conditions, the equation determining a nondimensional constant  $(k_n L)^2$  corresponding to the  $n$ th natural frequency is obtained as

$$\left[ (\alpha_1^*)^2 - \frac{1}{\lambda_0^2} \right] (\bar{k}_2 \cos \lambda_1 L - \bar{k}_1 \sin \lambda_1 L) + \left[ (\alpha_2^*)^2 + \frac{1}{\lambda_0^2} \right] (\sinh \lambda_2 L + \bar{k}_2 \cosh \lambda_2 L) = 0 \quad (135)$$

in which  $\bar{k}_1$  and  $\bar{k}_2$  are defined as

$$\bar{k}_1 = -\frac{\alpha_2^* + \frac{1}{\alpha_2^* \lambda_0^2}}{\alpha_1^* + \frac{1}{\alpha_1^* \lambda_0^2}} \quad (136)$$

$$\bar{k}_2 = -\frac{-\frac{\bar{k}_1}{\alpha_1^*} \cos \lambda_1 L + \frac{1}{\alpha_2^*} \cosh \lambda_2 L}{-\frac{1}{\alpha_1^*} \sin \lambda_1 L + \frac{1}{\alpha_2^*} \sinh \lambda_2 L} \quad (137)$$

The value of  $(k_n L)^2$  is determined from Eq. (135) as follows:

STEP 1. From Eqs. (113) and (114), determine  $\lambda_0^*$  and  $\lambda_0$ .

STEP 2. From Eq. (112), determine  $\hat{\lambda}_0$ .

STEP 3. Assume the value of  $(k_n L)^2$ .

STEP 4. From Eq. (120), determine  $\alpha$ .

STEP 5. From Eqs. (116) to (119), determine  $\lambda_1$ ,  $\lambda_2$ ,  $\alpha_1^*$  and  $\alpha_2^*$ , respectively.

STEP 6. From Eqs. (136) and (137), calculate  $\bar{k}_1$  and  $\bar{k}_2$ .

STEP 7. Substitute these values into Eq. (135) and find out the value of  $(k_n L)^2$  satisfying Eq. (135) with trial and error.

Hence, the value of  $(k_n L)^2$  depends on the slenderness ratios,  $\lambda_0^*$  and  $\lambda_0$ , of the uniform tube structure. So, for practical uses, the value of  $(k_n L)^2$  for the given values  $\lambda_0^*$  and  $\lambda_0$  can be presented previously as shown in Figure 21. Numerical results show that the values of  $(k_n L)^2$  depend mainly on  $\lambda_0$  and are negligible for the variation of  $\lambda_0^*$ . When  $\lambda_0$  increases, the value of  $(k_n L)^2$  approaches the value of the well-known Bernoulli-Euler beam. The practical tube structures take a value in the region from  $\lambda_0 = 0.1$  to  $\lambda_0 = 5$ .

Thus, substituting the value of  $(k_n L)^2$  into Eq. (111), the  $n$ th natural frequency,  $\omega_n$ , of the tube structure is

$$\omega_n = \frac{(k_n L)^2}{L^2} \sqrt{\frac{EI}{\rho A}} \quad (138)$$

Using Figure 21, the structural engineers may easily obtain from the first to tenth natural frequencies and also grasp the relationships among these natural frequencies.

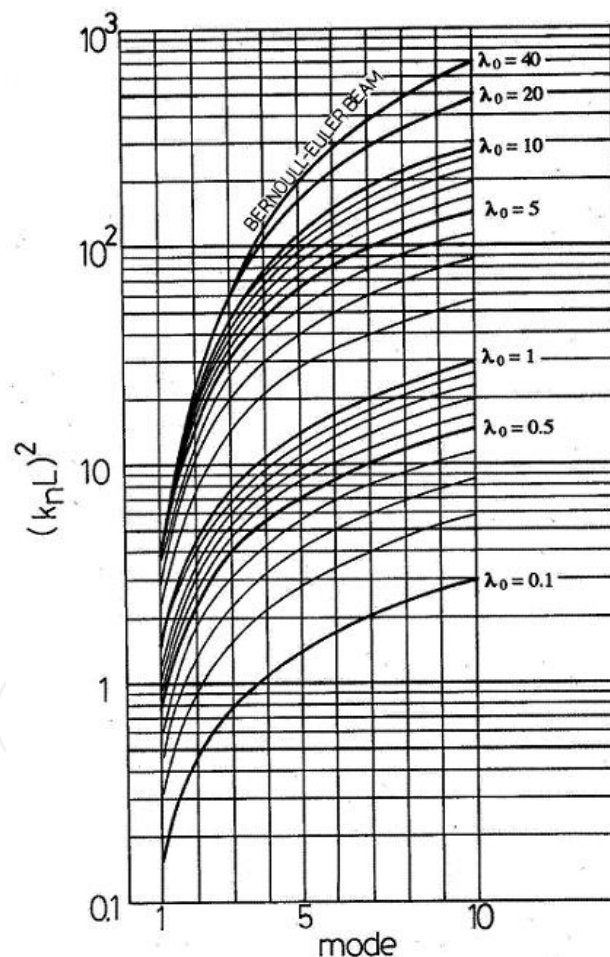
The  $n$ th natural function,  $\Phi_n$ , corresponding to the  $n$ th natural frequency is

$$\Phi_n(x) = -\bar{k}_2 \cos \lambda_1 x + \bar{k}_1 \sin \lambda_1 x + \sin h \lambda_2 x + \bar{k}_2 \cos h \lambda_2 \quad (139)$$

Now, neglecting the effect of the shear lag, the solutions proposed here agree with the results for a uniform Timoshenko beam presented by Herrmann [21] and Young [22].

### 7.3. Natural frequency of variable tube structures

The natural frequency of a uniform tube structure has been proposed in closed form. For a variable tube structure the proposed results give the approximate natural frequency by replacing the variable tube structure with a pseudo uniform tube structure having an appropriate reference stiffness.



**Figure 21.** Values of  $(k_n L)^2$  [3]

On the other hand, the natural frequency for a variable tube structure is presented by means of the Galerkin method. So, Eq. (108) may be rewritten as

$$EI\Phi''' - \omega^2 \left[ \rho A\Phi - \rho A \left( \frac{L}{\hat{\lambda}_0} \right)^2 \Phi'' \right] = 0 \quad (140)$$

$\Phi$  is expressed by a power series expansion as follows

$$\Phi(x) = \sum_{n=1}^{\infty} c_n \Phi_n \quad (141)$$

in which  $c_n$  = unknown coefficients; and  $\Phi_n(x)$  = functions satisfying the specified boundary conditions of the variable tube structure. Approximately,  $\Phi_n(x)$  take the natural function of the pseudo uniform tube structure, as given in Eq. (139). Applying Eq. (141) into Eq. (140), the Galerkin equations of Eq. (140) become

$$\delta c_m : \sum_{n=1}^{\infty} c_n (A_{mn} - \omega^2 B_{mn}) = 0 \quad (142)$$

in which the coefficients,  $A_{mn}$  and  $B_{mn}$ , are defined as

$$A_{mn} = \int_0^L EI \Phi_n''' \Phi_m dx \quad (143)$$

$$B_{mn} = \int_0^L \rho A \Phi_n \Phi_m dx - \int_0^L \rho A \left( \frac{L}{\hat{\lambda}_0} \right) \Phi_n''' \Phi_m dx \quad (144)$$

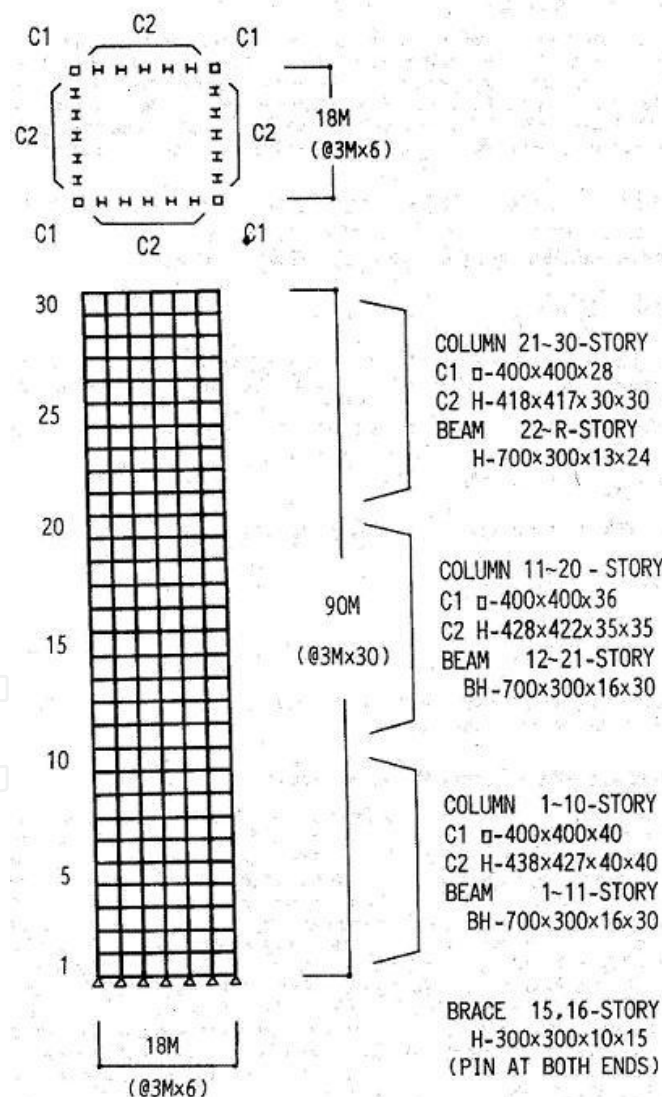
Hence, the natural frequency of the variable tube structure is obtained from solving eigenvalue problem of Eq. (142).

#### 7.4. Numerical results for natural frequencies

The natural frequencies for doubly symmetric uniform and variable tube structures have been presented by means of the analytical and Galerkin methods, respectively. In order to examine the natural frequencies proposed here, numerical computations were carried out for a doubly symmetric steel frame tube, as shown in Figure 22. This frame tube equals to the tube structure used in the static numerical example in the Section 6, except for with or without bracing at 15 and 16 stories. The data used are as follows: the total story is 30; each story height is 3 m; the total height,  $L$ , is 90 m; the base is rigid; Young's modulus  $E$  of the material used is  $2.05 \times 10^{11}$  N/m<sup>2</sup>. The weight per story is  $9.8 \text{ kN/m}^2 \times 18 \text{ m} \times 18 \text{ m} = 3214 \text{ kN}$ .

The cross sections of columns and beams in the variable frame tube shown in Figure 22 vary in three steps along the height. On the other hand, the uniform frame tube is assumed to be the stiffness at the midheight ( $L/2$ ) of the variable tube structure.

Table 7 shows the natural frequencies of the uniform and variable frame tubes, in which the approximate solution for the variable frame tube indicates the value obtained from replacing the variable frame tube with a pseudo uniform frame tube having the stiffnesses at the lowest story. The results obtained from the proposed method show excellent agreement with the three-dimensional frame analysis using FEM code NASTRAN. The approximate solution for the variable frame tube is also applicable to determine approximately the natural frequencies in the preliminary stages of the design.



**Figure 22.** Numerical model of frame tube [3]



NATURAL FREQUENCIES (rad/s)					
UNIFORM FRAME TUBE			VARIABLE FRAME TUBE		
Mode (1)	Analytical solution (2)	Frame theory (3)	Approximate solution (4)	Galerkin method (5)	Frame theory (6)
First	1.956	2.011	2.059	1.906	2.044
Second	5.907	6.196	6.218	6.203	6.141
Third	10.458	11.121	10.994	11.056	10.908
Fourth	14.708	15.822	15.460	15.341	15.683
Fifth	19.053	20.672	20.024	20.002	20.359

**Table 7.** Natural frequencies of uniform and variable frame tubes [3]

8. Expansion of one-dimensional extended rod theory

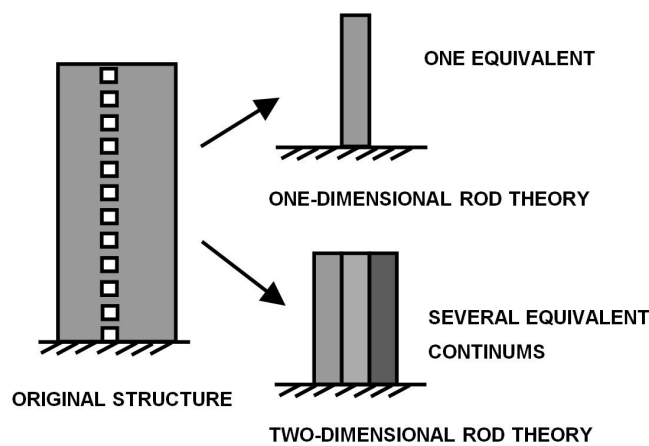
In order to carry out approximate analysis for a large scale complicated structure such as a high-rise building in the preliminary design stages, the use of equivalent rod theory is very effective. Rutenberg [10], Smith and Coull [23], Tarjan and Kollar [24] presented approximate calculations based on the continuum method, in which the building structure stiffened by an arbitrary combination of lateral load-resisting subsystems, such as shear walls, frames, coupled shear walls, and cores, are replaced by a continuum beam. Georgoussis [25] proposed to asses frequencies of common structural bents including the effect of axial deformation in the column members for symmetrical buildings by means of a simple shear-flexure model based on the continuum approach. Tarian and Kollar [24] presented the stiffnesses of the replacement sandwich beam of the stiffening system of building structures.

Takabatake et al. [2-6, 26-28] developed a simple but accurate one-dimensional extended rod theory which takes account of longitudinal, bending, and transverse shear deformation, as well as shear-lag. In the preceding sections the effectiveness of this theory has been demonstrated by comparison with the numerical results obtained from a frame analysis on the basis of FEM code NASTRAN for various high-rise buildings, tube structures and mega structures.

The equivalent one-dimensional extended rod theory replaces the original structure by a model of one-dimensional rod with an equivalent stiffness distribution, appropriate with regard to the global behavior. Difficulty arises in this modeling due to the restricted number of freedom of the equivalent rod; local properties of each structural member cannot always be properly represented, which leads to significant discrepancy in some cases. The one-dimensional idealization is able to deal only with the distribution of stiffness and mass in the longitudinal direction, possibly with an account of the averaged effects of transverse stiffness variation. In common practice, however, structures are composed of a variety of members or structural parts, often including distinct constituents such as a frame-wall or coupled wall with opening. Overall behavior of such a structure is significantly affected by the local distribution of stiffness. In addition, the individual behavior of each structural member

plays an important role from the standpoint of structural design. So, Takabatake [29, 30] propose two-dimensional extended rod theory as an extension of the one-dimensional extended rod theory to take into account of the effect of transverse variations in individual member stiffness.

Figure 23 illustrates the difference between the one- and two-dimensional extended rod theories in evaluating the local stiffness distribution of structural components. In the two-dimensional approximation, structural components with different stiffness and mass distribution are continuously connected. On the basis of linear elasticity, governing equations are derived from Hamilton's principle. Use is made of a displacement function which satisfies continuity conditions across the boundary surfaces between the structural components.



**Figure 23.** The difference between one- and two-dimensional rod theories [29]

Two-dimensional extended rod theory has been presented for simply analyzing a large or complicated structure such as a high-rise building or shear wall with opening. The principle of this theory is that the original structure comprising various different structural components is replaced by an assembly of continuous strata which has stiffness equivalent to the original structure in terms of overall behavior. The two-dimensional extended rod theory is an extended version of a previously proposed one-dimensional extended rod theory for better approximation of the structural behavior. The efficiency of this theory has been demonstrated from numerical results for exemplified building structures of distinct components. This theory may be applicable to soil-structure interaction problems involving the effect of multi-layered or non-uniform grounds.

On the other hand, the exterior of tall buildings has frequently the shape with many setback parts. On such a building the local variation of stress is considered to be very remarkable due the existence of setback. This nonlinear phenomenon of stress distribution may be explained by two-dimensional extended rod theory but not by one-dimensional extended rod theory. In order to treat exactly the local stress variation due to setback, the proper boundary condition in the two-dimensional extended rod theory must separate into two parts. One part is the mechanical boundary condition corresponding to the setback part and the

other is the continuous condition corresponding to longitudinally adjoining constituents. Thus, Takabatake et al. [30] proved the efficiency of the two-dimensional extended rod theory to the general structures with setbacks.

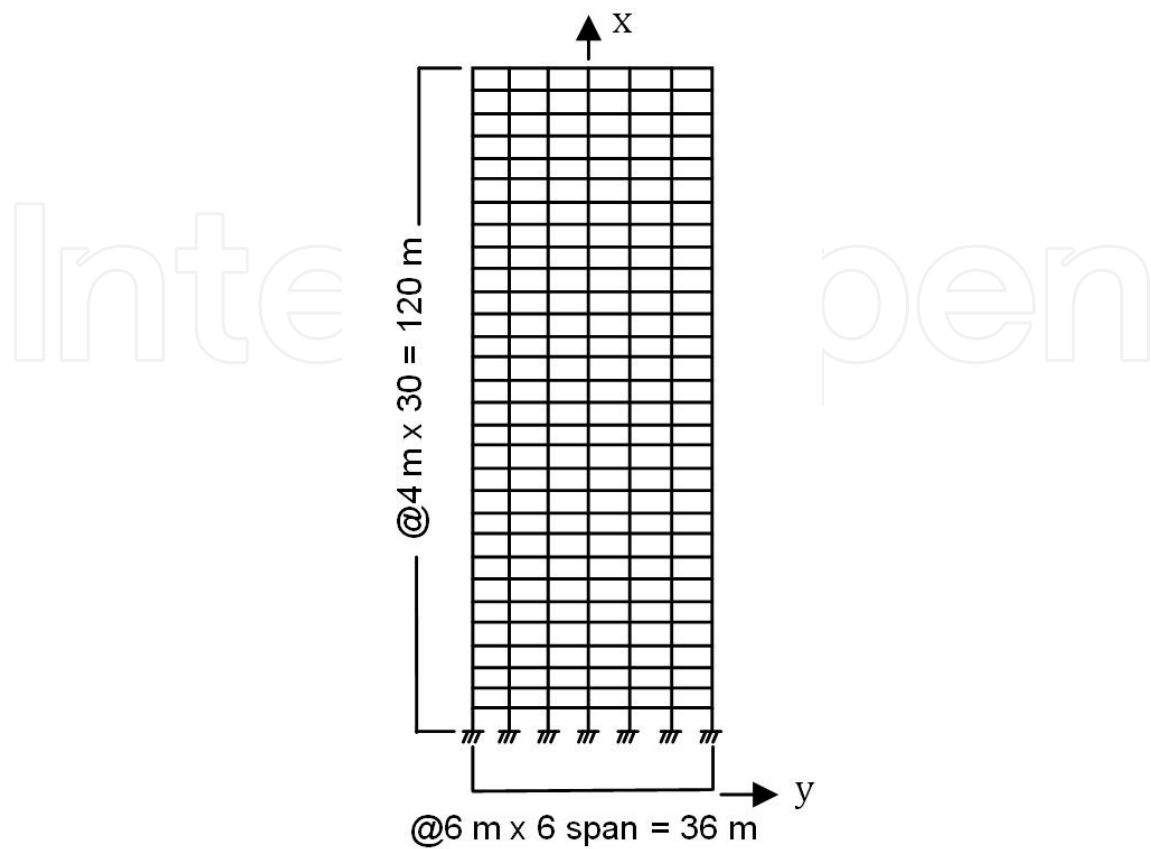
Two-dimensional extended rod theory has been presented for simply analyzing a large or complicated structure with setback in which the stiffness and mass due to the existence of setback vary rapidly in the longitudinal and transverse directions. The effectiveness of this theory has been demonstrated from numerical results for exemplified numerical models. The transverse-wise distribution of longitudinal stress for structures with setbacks has been clarified to behave remarkable nonlinear behavior. Since the structural form of high-rise buildings with setbacks is frequently adapted in the world, the incensement of stress distribution occurred locally due to setback is very important for structural designers. The present theory may estimate such nonlinear stress behaviors in the preliminary design stages. The further development of the present theory will be necessary to extend to the three-dimensional extended rod theory which is applicable to a complicated building with three dimensional behaviors due to the eccentric station of many earthquake-resistant structural members, such as shear walls with opening.

## 9. Current problem of existing high-rise buildings

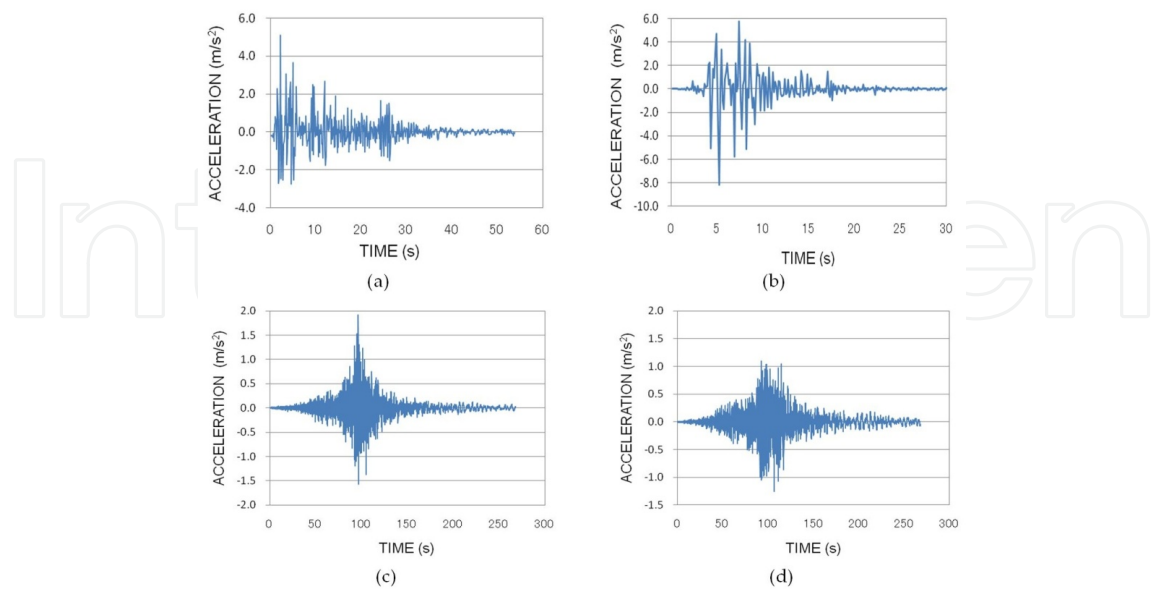
High-rise buildings have relative long natural period from the structural form. This characteristic is considered to be the most effective to avoid structural damages due to earthquake actions. However, when high-rise buildings subject to the action of the earthquake wave included the excellent long period components, a serious problem which the lateral deflection is remarkably large is produced in Japan. This phenomenon is based on resonance between the long period of high-rise buildings and the excellent long period of earthquake wave.

The 2011 Tohoku Earthquake (M 9.0) occurred many earthquake waves, which long period components are distinguished, on everywhere in Japan. These earthquake waves occur many physical and mental damages to structures and people living in high-rise buildings. The damage occurs high-rise buildings existing on all parts of Japan which appears long distance from the source. People entertain remarkable doubt about the ability to withstand earthquakes of high-rise buildings. This distrust is an urgent problem to people living and working in high-rise buildings. Existing high-rise buildings are necessary to improve urgently earthquake resistance. This section presents about an urgency problem which many existing high-rise buildings face a technical difficulty.

Let us consider dynamic behavior for one plane-frame of a high-rise building, as shown in Figure 24.



**Figure 24.** Numerical model



**Figure 25.** Time histories of acceleration (a) EL-Centro 1940 NS, (b) JMA Kobe 1995 NS, (c) Shinjuku 2011 NS, and (d) Urayasu 2011 NS

This plane frame is composed of uniform structural members. The sizes of columns and beams are □-800 x 800 x 25 (BCP) and H-400 x 300 x 11 x 18 (SN400B), respectively. The inertia moment of beams takes twice due to take into account of slab stiffness. This plane frame is a part of a three-dimensional frame structure with the span 6 m between adjacent plane-frames. The width and height are 36 m and 120 m, respectively. The main data used in numerical calculations are given in Table 8. Four kinds of earthquake waves are given in Table 9. El-Centro 1940 NS is converted the velocity to 0.5 m/s; JMA Kobe 1995 NS is the original wave with the maximum velocity 0.965 m/s; Shinjuku 2011 NS is the original wave with the maximum velocity 0.253 m/s; and Urayasu 2011 NS is the original wave with the maximum velocity 0.317 m/s. Figures 25(a) to 25(d) indicate time histories of accelerations for the four earthquake waves. In these earthquake waves, Shinjuku 2011 NS and Urayasu 2011 NS are obtained from K-net system measured at the 2011 Tohoku Earthquake. These earthquake waves are considered as earthquake waves included the excellent long periods. The excellent periods obtained from the Fourier spectrum of Shinjuku 2011 NS and Urayasu 2011 NS earthquake waves are 1.706 s and 1.342 s, respectively. The maximum acceleration and maximum velocity of these earthquake waves are shown in Table 9.

Structure shape	Width:	@6 m x 6 = 36 m
	Height:	@4 m x 30 floors = 120 m
Weight per floor (kN/m <sup>2</sup> )	12	
Young modulus <i>E</i> (N/m <sup>2</sup> )	2.06 x 10 <sup>11</sup>	
Shear modulus <i>G</i> (N/m <sup>2</sup> )	7.92 x 10 <sup>10</sup>	
Mass density <i>ρ</i> (N/m <sup>3</sup> )	7850	
Damping constant	0.02	
Poisson ratio	0.3	

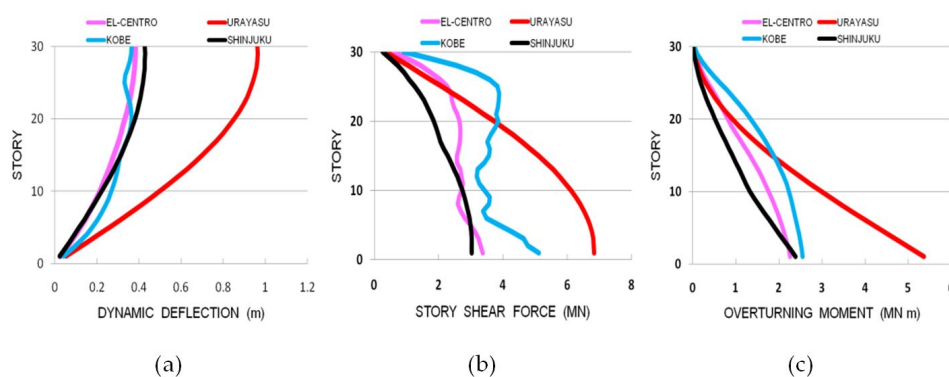
**Table 8.** Main data for numerical model

Figure 26(a) shows the dynamic maximum lateral displacement subjected to the four kinds of earthquake waves. The maximum dynamic lateral displacement subject to Urayasu 2011 NS is remarkable larger than in the other earthquake waves. Figures 26(b) and (c) indicate the maximum shear force and overturning moment of the plane high-rise building subject to these earthquake actions, respectively. Earthquake wave Urayasu 2011 NS which includes long period components influence remarkable dynamic responses on the current high-rise building.

Earthquake Wave	Maximum Acceleration	Maximum Velocity
	m/s <sup>2</sup>	m/s
EL-CENTRO 1940 NS	5.11	0.500
JMA KOBE 1995 NS	8.18	0.965
SHINJUKU 2011 NS	1.92	0.253
URAYASU 2011 NS	1.25	0.317

**Table 9.** Maximum acceleration and maximum velocity of each earthquake wave

It is very difficult to sort out this problem. If the existing structure stiffens the transverse shear rigidity of overall or selected stories, the dynamic responses produced by the earthquake wave included excellently long period decrease within initial design criteria for dynamic calculations. However, inversely the dynamic responses produced by both EL-Centro 1940 NS with the maximum velocity 0.5 m/s and JMA Kobe 1995 NS exceed largely over the initial design criteria. The original design is based on flexibility which is the most characteristic of high-rise buildings. This flexibility brings an effect which lowers dynamic responses produced by earthquake actions excluding long period components. Now, changing the structural stiffness from relatively soft to hard, this effect is lost and the safety of the high-rise building becomes dangerous for earthquake waves excluding the long period components.



**Figure 26.** Distribution of dynamic responses (a) dynamic lateral deflection, (b) story shear force, and (c) overturning moment

Author has not in this stage a clear answer to this problem. This problem includes two situations. The first point is to find out the appropriate distribution of the transverse stiffness. The variation of the transverse stiffness is considered to stiffen or soften. In general, existing high-rise buildings are easily stiffening then softening. However, there is a strong probability that the stiffening of the transverse shear stiffness exceeds the allowable limit for the lateral deflection, story shear force, and overturning moment in the dynamic response subjected to earthquake waves used in original structural design. Therefore, the softening of the transverse shear stiffness used column isolation for all columns located on one or more selected story is considered to be effective. It is clarified from author's numerical computations that the isolated location is the most effective at the midheight. The second point is to find out an effective seismic retrofitting to existing high-rise buildings without the movement of people living and working in the high-rise building. These are necessary to propose urgently these measures for seismic retrofitting of existing high-rise buildings subject to earthquake waves included excellently long wave period. This subject will be progress to ensure comfortable life in high-rise buildings by many researchers.



## 10. Conclusions

A simple but accurate analytical theory for doubly symmetric frame-tube structures has been presented by applying ordinary finite difference method to the governing equations proposed by the one-dimensional extended rod theory. From the numerical results, the present theory has been clarified to be usable in the preliminary design stages of the static and dynamic analyses for a doubly symmetric single or double frame-tube with braces, in practical use. Furthermore, it will be applicable to hyper high-rise buildings, e.g. over 600m in the total height, because the calculation is very simple and very fast. Next the approximate method for natural frequencies of high-rise buildings is presented in the closed-form solutions. This method is very simple and effective in the preliminary design stages. Furthermore, the two-dimensional extended rod theory is introduced as for the expansion of the one-dimensional extended rod theory. Last it is stated to be urgently necessary seismic retrofitting for existing high-rise buildings subject to earthquake wave included relatively long period.

## Author details

Hideo Takabatake\*

Address all correspondence to: hideo@neptune.kanazawa-it.ac.jp

Department of Architecture, Kanazawa Institute of Technology, Institute of Disaster and Environmental Science, Japan

## References

- [1] Reissner, E. (1946). Analysis of shear lag in box beams by the principle of minimum potential energy. *Quarterly of Applied Mathematics*, 4(3), 268-278.
- [2] Takabatake, H., Mukai, H., & Hirano, T. (1993). Doubly symmetric tube structures- I: Static analysis. *Journal of Structural Engineering ASCE*, 119(7), 1981-2001.
- [3] Takabatake, H., Mukai, H., & Hirano, T. (1993). Doubly symmetric tube structures- II: Static analysis. *Journal of Structural Engineering ASCE*, 119(7), 2002-2016.
- [4] Takabatake, H., Mukai, H., & Hirano, T. (1996). Erratum for "Doubly symmetric tube structures- I: Static analysis. *Journal of Structural Engineering ASCE*, 122(2), 225.
- [5] Takabatake, H., Takesako, R., & Kobayashi, M. (1995). A simplified analysis of doubly symmetric tube structures. *The Structural Design of Tall Buildings*, 4(2), 137-153.
- [6] Takabatake, H. (1996). A simplified analysis of doubly symmetric tube structures by the finite difference method. *The Structural Design of Tall Buildings*, 5(2), 111-128.

- [7] Beck, H. (1962). Contribution to the analysis of coupled shear walls. *Journal of the American Concrete Institute*, 59(8), 1055-1069.
- [8] Heidenbrech, A. C., & Smith, B. S. (1973). Approximate analyses of tall wall-frame structures. *Journal of the Structural Division ASCE*, 99(2), 199-221.
- [9] Tso, W. K., & Chan, H. (1971). Dynamic analysis of plane coupled shear walls. *Journal of Engineering Mechanics Division ASCE*, 97(1), 33-48.
- [10] Rutenberg, A. (1975). Approximate natural frequencies for coupled shear walls. *Earthquake Engineering and Structural Dynamics*, 4(1), 95-100.
- [11] Rutenberg, A. (1977). Dynamic properties of asymmetric wall-frame structures. *Earthquake Engineering and Structural Dynamics*, 5(1), 41-51.
- [12] Danay, A., Gluck, J., & Geller, M. (1975). A generalized continuum method for dynamic analysis of asymmetric tall buildings. *Earthquake Engineering and Structural Dynamics*, 4(2), 179-203.
- [13] Bause, A. K., Nagpal, A. K., Bajaj, R. S., & Guiliani, A. K. (1979). Dynamic characteristics of coupled shear walls. *Journal of the Structural Division ASCE*, 105(8), 1637-1652.
- [14] Cheung, Y. K., & Swaddiwudhipong, S. (1979). Free vibration of frame shear wall structures on flexible foundations. *Earthquake Engineering and Structural Dynamics*, 7(4), 355-367.
- [15] Coull, A., & Smith, B. S. (1973). Torsional analyses of symmetric structures. *Journal of the Structural Division ASCE*, 99(1), 229-233.
- [16] Coull, A., & Bose, B. (1975). Simplified analysis of frame-tube structures. *Journal of the Structural Division ASCE*, 101(11), 2223-2240.
- [17] Smith, B. S., Kuster, M., & Hoenderkamp, J. C. D. (1984). Generalized method for estimating drift in high-rise structures. *Journal of Structural Engineering ASCE*, 110(7), 1549-1562.
- [18] Smith, B. S., & Crowe, E. (1986). Estimating periods of vibration of tall buildings. *Journal of Structural Engineering ASCE*, 112(5), 1005-1019.
- [19] Paz, M. (2006). *Structural Dynamics*. , 3rd Edn. Van Nostrand Reinhold New York., 74-75.
- [20] Craig, R. R. (1981). *Structural dynamics*. John Wiley and Sons, New York.
- [21] Herrmann, G. (1955). Forced motions of Timoshenko beams. *J. Appl. Mech. Trans. ASME*, 22(2), 53-56.
- [22] Young, D. (1962). *Continuos systems: Handbook of engineering mechanics*. , W. Flügge, ed., McGraw-Hill. New York, N.Y. , 1-34.
- [23] Smith, B. S., & Coull, A. (1991). *Tall building structures: analysis and design*.. John Willy & Sons, New York.



- [24] Tarjian, G., & Kollar, L. P. (2004). Approximate analysis of building structures with identical stories subjected to earthquake. *International Journal of Solids and Structures*, 41(5), 1411-1433.
- [25] Georgoussis, G. K. (2006). A simple model for assessing periods of vibration and modal response quantities in symmetrical buildings. *The Structural Design of Tall and Special Buildings*, 15(2), 139-151.
- [26] Takabatake, H., & Nonaka, T. (2001). Numerical study of Ashiyahama residential building damage in the Kobe Earthquake. *Earthquake Engineering and Structural Dynamics*, 30(6), 879-897.
- [27] Takabatake, H., Nonaka, T., & Tanaki, T. (2005). Numerical study of fracture propagating through column and brace of Ashiyahama residential building in Kobe Earthquake. *The Structural Design of Tall and Special Buildings*, 14(2), 91-105.
- [28] Takabatake, H., & Satoh, T. (2006). A simplified analysis and vibration control to super-high-rise buildings. *The Structural Design of Tall and Special Buildings*, 15(4), 363-390.
- [29] Takabatake, H. (2010). Two-dimensional rod theory for approximate analysis of building structures. *Earthquakes and Structures*, 1(1), 1-19.
- [30] Takabatake, H., Ikarashi, F., & Matsuoka, M. (2011). A simplified analysis of super building structures with setback. *Earthquakes and Structures*, 2(1), 43-64.